

# On The Detection of Artefacts in Spectro-Astrometry

E.Brannigan<sup>1\*</sup>, M. Takami<sup>1,2</sup>, A. Chrysostomou<sup>1</sup>, J. Bailey<sup>3</sup>

<sup>1</sup>*Centre for Astrophysics Research, University of Hertfordshire, Hatfield, HERTS AL10 9AB, UK*

<sup>2</sup>*Subaru Telescope, 650 North A'ohoku Place, Hilo, HI 96720, USA*

<sup>3</sup>*Anglo-Australian Observatory, PO Box 296, Epping, NSW 1710, Australia*

Accepted 2005 ??. Received ????; in original form ????

## ABSTRACT

We demonstrate that artificial bipolar structure can be detected using spectro-astrometry when the point spread function (PSF) of a point source suffers distortion in a relatively wide slit. Spectro-Astrometry is a technique which allows us to probe the spatial structure of astronomical sources on milliarcsecond (mas) scales making it possible to detect close binaries and to study the geometry and kinematics of outflowing gas on scales much smaller than the seeing or the diffraction limit of the telescope. It is demonstrated that distortion of the PSF, caused by tracking errors of the telescope or unstable active optics during an exposure can induce artificial signals which may be misinterpreted as a real spectro-astrometric signal. Using simulations we show that these may be minimised by using a narrow slit relative to the seeing. Spectra should be obtained at anti-parallel slit position angles (e.g.,  $0^\circ$  and  $180^\circ$ ) for comparison in order to allow artificial signatures to be identified.

**Key words:** Spectro-Astrometry Line: Formation Line: Profiles Stars: Pre-Main Sequence ISM: Jets and Outflows.

## 1 INTRODUCTION

Spatial resolutions of optical-IR facilities have dramatically improved over the last decade. Indeed, the *Hubble Space Telescope* and adaptive optics on ground based 8-10m telescopes have provided spatial resolutions of 0.05 arcseconds, leading to a better understanding of the nature of a variety of astronomical objects. Despite this, even higher spatial resolutions are desired to study the geometry of extrasolar planetary systems, populations and formation of close binaries, mechanisms of mass ejection and accretion in young and evolved stars and the nature of active galactic nuclei. Optical-IR interferometry has begun to provide resolutions on milliarcsecond (mas) scales, however its applicability is limited due to the complexity of the technique.

Spectro-astrometry is an alternative approach to study milliarcsecond structures at optical-IR wavelengths. The basic concept is to measure the relative position of the source as a function of wavelength using either an intensity weighted centroiding algorithm or profile fitting (see Bailey 1998a for a more detailed description). The resultant “position spectrum” will show structure on any spectral feature that is displaced from the centroid of the continuum source: e.g., an emission line arising in a binary companion, outflowing jets or any other structure that is not perfectly symmetric about the centroidal source, or whose displacement from the

source varies with wavelength. The smallest spatial scale observed is limited by the seeing or the diffraction limit of the telescope, however this technique indeed provides astronomically useful information at spatial scales much smaller than these.

The concept was introduced in the 1980’s as “Differential Speckle Interferometry” or “Chromatic Position Difference” (e.g., Beckers 1982), and demonstrated to detect close binaries (e.g., Sorokin & Tokovinin 1985). This broad band technique was limited by the necessity to correct for atmospheric dispersion which can be much larger than the observed structure. This difficulty is removed by measuring the displacement of a spectral line at high resolution. Aime et al. (1988) were able to measure spectro-astrometric structure using special instrumentation. See Bailey (1998a) for review of these works.

More recently Bailey (1998a) adapted this technique using a standard long-slit CCD spectrograph and coined the term “spectro-astrometry”. The method is similar to that used by Solf & Böhm (1993), who studied a jet from a young stellar object (YSO) on subarcsecond/arcsecond scales. Bailey (1998a) revised this method and has shown that with good spatial uniformity of the CCD coupled with a pixel scale that allows excellent sampling of the seeing profile positional accuracies as small as 1mas are achieved (see Takami 2003). Bailey has also shown that the technique is a powerful tool for discovering binary companions toward young and evolved stars, separating their spectra, and study-

\* E-mail: e.brannigan@star.herts.ac.uk

ing the kinematics of YSO jets/winds and narrow line regions of active galactic nuclei (AGN). Since this method doesn't require any special instrumentation, its popularity has steadily increased in recent years. Studies made for young binaries and YSO jets include Bailey(1998b), Takami et.al. (2001,2002,2003), Davis et al. (2001,2003), Whelan, Ray & Davis(2004) and Baines et al. (2004). Measurements using an integral field unit (IFU) were first conducted by Garcia, Thiébaud & Bacon (1999). A similar approach using VLTI-AMBER is investigated by Petrov (2003), Marconi et al. (2003) and Dougados et al. (2003). Since the positional accuracy achieved depends on the PSF size as well as the photon noise, using an interferometer for this approach has the potential to achieve information on spatial structures at *microarcsecond* scales (Bailey 1998a).

Instrumental effects which may compromise spectro-astrometric observations have not been fully investigated. These effects may indeed create false detections of close binaries or bipolar outflows. Possible instrumental effects include; misalignment of the spectrum with CCD columns, any departure of the CCD pixels from a regular grid, imperfect flatfielding or charge transfer deficiencies in the CCD (Bailey 1998b; Takami et al. 2001). To eliminate instrumental effects, Bailey (1998a,b) proposed to obtain position spectra at anti-parallel slit position angles (e.g.,  $0^\circ$  and  $180^\circ$ ) via rotation of the instrument. On comparison of these spectra, any real signal from the object will change sign, while the instrumental effects remain constant. We can thus eliminate instrumental effects by subtracting one position spectrum from the other. This method is followed by Takami et al. (2001,2002,2003) and Baines (2004). Garcia et al. (1999), Davis et al. (2001,2003) and Whelan et al. (2004) however eliminate instrumental effects by polynomial fitting of the continuum position.

Bailey (1998a) reports a systematic effect upon observation of sharp unresolved lines. This is caused by either telescope tracking errors or unstable active optics during the exposure, and appears in the position spectrum as a P Cygni type profile. Bailey warns that the target spectral lines should be well resolved to observe true positional displacement. This instrumental effect could be eliminated in some cases by Bailey's method, but this cannot be done by polynomial fitting of the continuum position. In this paper we show that this instrumental effect can appear even if the line profile is fully resolved as was the case in position spectra of RU Lupi, obtained using the 3.5m New Technology Telescope (NTT). Takami et al. had previously detected the presence of bipolar outflow in this object using the 3.9m Anglo-Australian Telescope (AAT). Indeed the observed positional displacement in the NTT looks similar to that seen in the AAT data. We show that the signal detected in the NTT data is not real, motivating us to investigate the effect of uneven illumination on spectro-astrometry, how to avoid it and whether previously detected bipolar outflows are in fact real.

In §2 we describe the spectro-astrometric observations obtained using EMMI on the 3.6m NTT and the results in which artificial signatures were detected. These artefacts are identified by qualitatively inspecting position spectra obtained using anti-parallel slit position angles. In §3 we (1) show that the observed position spectra are explained by distortion/motion of the stellar image in a relatively wide

slit, (2) show that the extent of the artefacts, in a given set of observing conditions, can be greatly reduced by using a slit width narrow in comparison to the seeing, and (3) show an example of the effect these artefacts have on real spectro-astrometric data. In §4 we give some recommendations on how to monitor the data for the false signatures of bipolar structure. In Appendix A, we show that the bipolar outflows reported by Takami et al. (2001,2003) are real and not due to the instrumental effect described here.

## 2 OBSERVATIONS AND RESULTS

Medium resolution spectroscopy of RU Lup was obtained with the 3.5m NTT in the early morning of April 8 2004, when the seeing was measured to be  $0.8''$ . The observations were made using the REad Medium Dispersion (REMD) mode of the ESO Multi-Mode Instrument (EMMI) with the #6 grating and an arcsecond slit. The wavelength coverage spanned 6100 to 6800Å with resolving power = 5000. The spectra were obtained at 4 position angles:  $0^\circ, 90^\circ, 180^\circ, 270^\circ$  by rotating the instrument. HeAr lamp spectra were used to calibrate the wavelength scale and a pixel scale of  $0.165''$  with the MIT detector provided good sampling of the seeing profile. Flat fields were obtained by combining many exposures of the spectrograph illuminated by a halogen lamp.

The data were reduced using the FIGARO package provided by Starlink, following Bailey (1998a,b) and Takami (2001,2003). After subtracting the bias level and flat-fielding, "position spectra" were determined by fitting the seeing profile at each wavelength with a gaussian function. Global instrumental effects in the position spectra are removed by polynomial fitting. This allows us to see the positional displacement of any emission/absorption features at each slit angle relative to the continuum. In addition to the position spectra, the intensity spectra were obtained by subtracting the bias, flat-fielding, subtracting the adjacent sky and extracting bright columns on the CCD.

The spectrum of RU Lup shows a wealth of emission lines as observed by Lago & Penston (1982) and Takami (2001). The intensity and position spectra of the  $H\alpha$   $\lambda 6563\text{\AA}$ , HeI  $\lambda 6678\text{\AA}$  & [SII]  $\lambda 6731\text{\AA}$  emission lines and LiI  $\lambda 6708\text{\AA}$  absorption line, obtained using EMMI-NTT, are shown in Figure 1. The  $H\alpha$  emission line shows a large offset in the position spectrum,  $\sim 25\text{mas}$  from the continuum position and the blue and red shifted wings are displaced in different directions. Similar displacement in  $H\alpha$  is reported in Takami (2001). Such structure usually indicates the presence of a bipolar outflow (see Appendix A). However a qualitative inspection of position spectra, obtained using anti-parallel slits (i.e.  $0^\circ$  &  $180^\circ$ ) in this data, reveals that the displacement seen in anti-parallel position spectra have equal sign indicating that the signature must be systematic. In addition, the displacement observed with slit position angle  $0^\circ$  is less than that observed with position angle  $180^\circ$ . In fact two position spectra observed at a position angle of  $0^\circ$  exhibit dissimilar profiles indicating that the effect responsible for the spurious displacement signal is time variable and as such cannot be removed even by obtaining position spectra at anti-parallel slit angles.

In addition to  $H\alpha$   $\lambda 6563\text{\AA}$  and HeI  $\lambda 6678\text{\AA}$ , evidence for

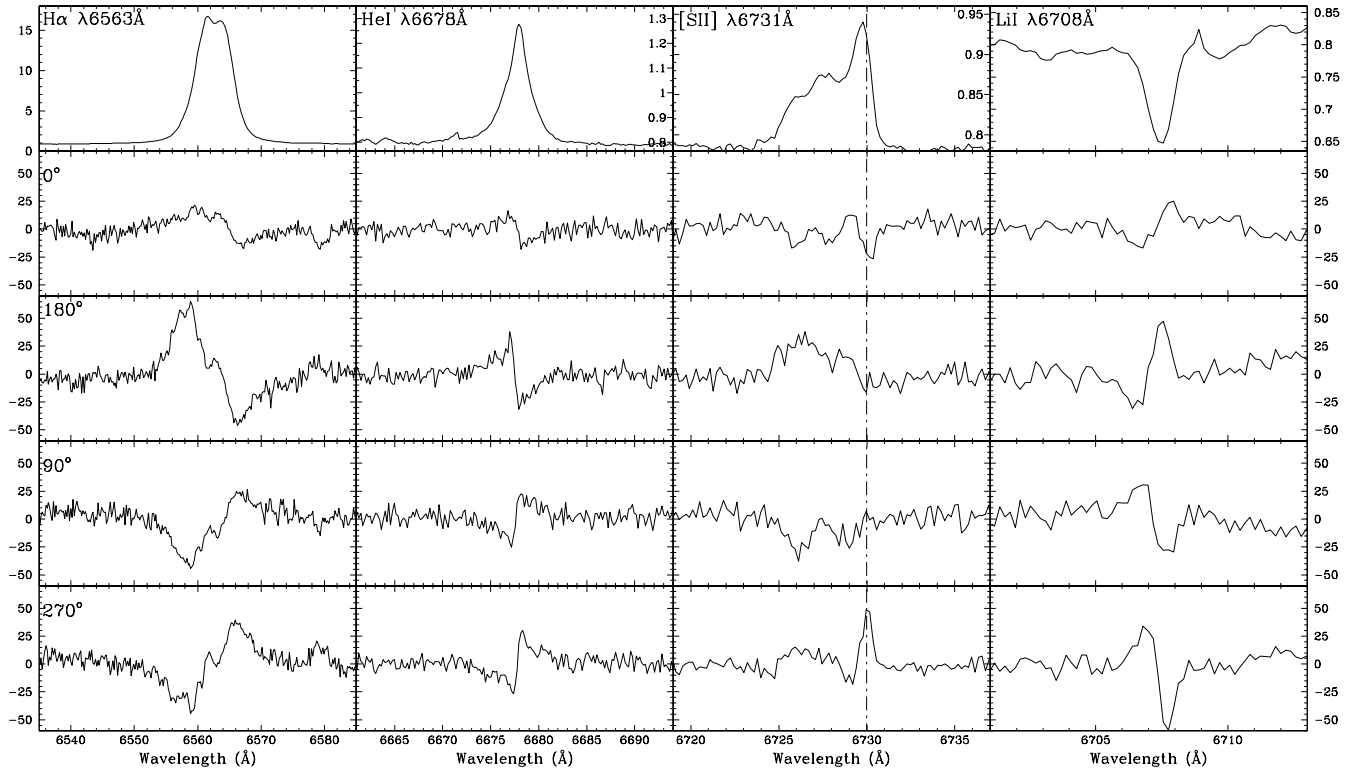


**Figure 1.** Intensity and position spectra of RU Lup obtained using EMMI-NTT. From left to right; Top:  $\text{H}\alpha$   $\lambda 6563\text{\AA}$ ,  $\text{HeI}$   $\lambda 6678\text{\AA}$  &  $[\text{SII}]$   $\lambda 6731\text{\AA}$  emission and  $\text{LiI}$   $\lambda 6708\text{\AA}$  absorption lines. The intensities shown are arbitrary; Lower four panels: spectro-astrometric signal (mas) for each corresponding spectral feature detected at 4 position angles  $0^\circ$ ,  $180^\circ$ ,  $90^\circ$  &  $270^\circ$  in the spectrum of RU Lup. The bottom two panels show position spectra for anti-parallel slit angles  $90^\circ$  &  $270^\circ$  in each of the spectral features, similarly in the third and fourth panels from the bottom position spectra for anti-parallel slit angles  $0^\circ$  &  $180^\circ$  in each of the spectral features is shown. In the blue wing of  $[\text{SII}]$   $\lambda 6731\text{\AA}$  emission feature the angular displacement is seen to change sign in corresponding anti-parallel slits, whereas displacement near zero velocity of the  $[\text{SII}]$   $\lambda 6731\text{\AA}$  line (marked with a dot-dashed line), in the permitted emission lines and the  $\text{LiI}$   $\lambda 6708\text{\AA}$  absorption line does not change sign in anti-parallel slits.

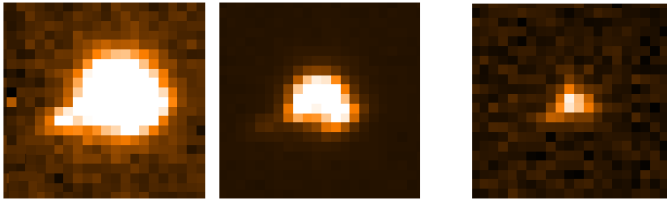


**Figure 2.** Image capture in slit viewer 7/4/2004 using 3.5m NTT. Pixel scale:  $0.4''$ . Left and Centre: distorted image of the Classical T Tauri Star (CTTS) SZ68. Right: distorted image of the CTTS SZ69

bipolar structure is seen in other bright permitted lines including  $\text{FeII}$   $\lambda 6238/6248/6456/6516\text{\AA}$ . The  $\text{LiI}$   $\lambda 6708\text{\AA}$  absorption line exhibits displacement similar to that of  $\text{H}\alpha$  and the bright permitted emission lines, although in any given spectrum the direction of displacement in  $\text{LiI}$  absorption is of opposite sign to that of the emission lines. For example, at a position angle of  $180^\circ$  the blue and redshifted components of the bright permitted emission lines show positive and negative displacement respectively, whereas the  $\text{LiI}$  absorption line shows negative and positive displacement in the blue and red wings respectively.

Conversely, the direction of displacement due to

blueshifted forbidden line emission reverses sign at anti-parallel slit positions ( $0^\circ$  vs.  $180^\circ$ ;  $90^\circ$  vs.  $270^\circ$ ). This is best seen in the  $[\text{SII}]$   $\lambda 6731\text{\AA}$  emission line in Figure 1. However a large, sharp displacement is observed close to zero velocity in the position spectrum at both  $[\text{SII}]$   $\lambda 6731\text{\AA}$  and  $[\text{OI}]$   $\lambda 6300\text{\AA}$  emission lines. This displacement is observed in all the position spectra for  $[\text{SII}]$   $\lambda 6731\text{\AA}$  (marked in Figure 1 with a dot-dashed line) and  $[\text{OI}]$   $\lambda 6300\text{\AA}$ . This sharp displacement does not reverse sign in anti-parallel slit position angles and therefore this is likely to be due to instrumental effects and not to actual signal from the object.

### 3 INDUCED SIGNAL DUE TO A DISTORTED STELLAR IMAGE IN A WIDE SLIT

The instrumental effects described in §2 were not observed in previous observing runs at the AAT described in Takami et al. (2001,2003). There are a number of key differences between these earlier observations and those reported in §2. Primarily, the typical seeing conditions differ dramatically ( $0.8''$  and  $1.5''/2.0''$ ) while a wide slit of  $1.0''$  was used in

<sup>1</sup> not shown as the effect in this line is the same as that in the  $[\text{SII}]$  line, but the data at the wavelength of  $[\text{OI}]$  is of lower quality

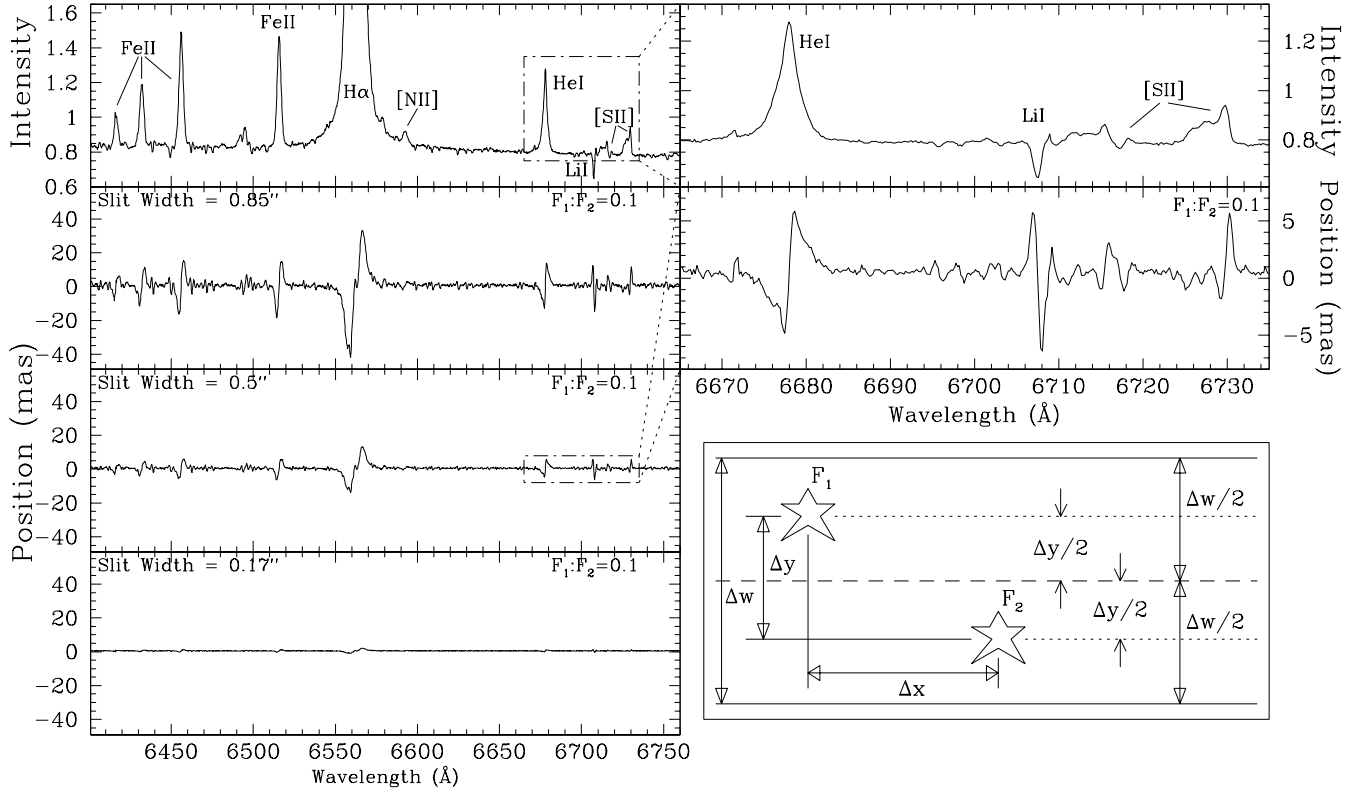


**Figure 3.** Top left: Intensity spectrum of RU Lup obtained on 8/4/2004 using EMMI on the 3.6m NTT. Lower left: simulated position spectra for a distorted PSF using 3 slit widths, 0.85'', 0.5'' & 0.17'', flux ratio  $F_1 : F_2 = 0.1$  and two point sources located off centre of the slit with identical spectra. Lower right: geometry used in the simulations to show that a distorted PSF can reproduce well the artefacts seen in the data. Top right: Close up view of the HeI, [SII] and LiI emission and absorption lines. Lower top right: positional displacement due to HeI, [SII] and LiI obtained from the simulations, where  $F_1 : F_2 = 0.1$  and slit width = 0.5''. The simulated displacement is similar to that seen in the data.

all of the observations. These artefacts are seen in observations when the seeing is smaller than the slit width used. Secondly, the stellar image suffered intermittent distortion during the later observations, as shown in Figure 2, due to an unstable active optics system. In §3.1 it is explained how these combined effects can induce an artificial signal in the position spectrum, and the extent of the artefacts that can be expected to occur for a given set of observing conditions is investigated. In §3.2 an example of the effect these artefacts can have on real spectro-astrometric signal is simulated.

### 3.1 Concepts and Simulations

When the intensity distribution from a given source is non-uniform across the slit the resultant spectrum can be slightly blue or redshifted. This blue/redshifted emission due to “uneven illumination” or “inaccurate centering”, (e.g., Bacciotti et al. 2002; Ardila et al. 2002) arises from an offset of the light source from the center of the slit, resulting in a deviation of the angle of incidence according to  $d\alpha = dy/f_{col}$ , where  $f_{col}$  is the focal length of the collimator. According to the grating equation:

$$m\lambda = (\sin \alpha \pm \sin \beta) \quad (1)$$

where  $m$  is the diffracted order,  $\lambda$  the diffracted wavelength,  $\alpha$  is the angle of incidence wrt. the normal and  $\beta$  the angle of diffraction wrt. the normal, this leads to a subsequent

deviation in the angle of diffraction which in turn is translated to a shift in the spectrum. Therefore, the shift in the spectrum,  $d\lambda$ , is proportional to the position of the light source from the center of the slit axis  $dy$ ;  $d\lambda = \text{const.} \times dy$ . This constant value can be readily determined from the spectral resolution of the instrument. For the REMD mode of EMMI-NTT a 1.0'' slit provides  $R = 5000$ , corresponding to  $\Delta\lambda = 1.2\text{\AA}$  giving us the relation:

$$d\lambda [\text{\AA}] = 1.2 \times dy [\text{arcsec}] \quad (2)$$

As such, if a stellar image is distorted or elongated in the slit, perhaps due to tracking errors of the telescope or unstable active optics, the spectrum close to the edges of the slit is slightly blue or redshifted. This geometry would be replicated by a bipolar outflow located within the slit. In order to determine the affect of these artefacts on spectro-astrometric observations simplified simulations of two point sources were carried out with their positions as depicted in Figure 3. Given that the point sources have spectra  $F_1 f(\lambda)$  and  $F_2 f(\lambda)$ , where  $F_1$  and  $F_2$  are constant and  $f(\lambda)$  is a normalised spectrum, the spectra are recorded at the detector as  $F_1 f(\lambda + \Delta\lambda)$  and  $F_2 f(\lambda - \Delta\lambda)$ . Thus the centroidal position at each wavelength is given by:

$$X_{cent}(\lambda) = \frac{\Delta x}{2} \times \frac{F_1 f(\lambda + 1.2\Delta y) - F_2 f(\lambda - 1.2\Delta y)}{F_1 f(\lambda + 1.2\Delta y) + F_2 f(\lambda - 1.2\Delta y)} \quad (3)$$

Parameter	Description	Distortion	Binary	Binary & Distortion
PS	Pixel Scale	0.17	0.17	0.17
$\lambda_{min}$	start wavelength	6100	6100	6100
$\lambda_{max}$	end wavelength	6850	6850	6850
$PA_{bin}$	Binary position angle	—	45°	45°
$\Delta S_{bin}$	Binary separation	—	0.1''	0.1''
F <sub>1</sub>	Flux of primary binary component	1.0	3.0	3.0
F <sub>2</sub>	Flux of secondary binary component	—	1.0	1.0
F <sub>distort</sub>	Percentage of flux in distortion	0.1 - 0.9	—	0.1 - 0.9
PA <sub>distort</sub>	Distortion position angle	135°	—	135°
$\Delta S_{distort}$	Distance between distortion and “real image”	0.1'' - 1.0''	—	0.1'' - 1.0''
FWHM	Gaussian simulated seeing	0.2'' - 1.7''	0.2'' - 1.7''	0.2'' - 1.7''
$\Delta w$	Slit width	0.1'' - 1.4''	0.1'' - 1.4''	0.1'' - 1.4''

**Table 1.** Parameters used in the simulations.

To confirm that the artefacts seen in this data are a result of uneven illumination of the slit simulations of a distorted PSF were carried out and position spectra obtained using equation (3), and the geometry described in Figure 3. The simulations reproduce a number of the artefacts observed in the data (Figure 1), specifically (see Figure 3): (1) evidence for bipolar structure exists in the bright permitted emission lines; (2) displacement seen at the Li I  $\lambda 6708\text{\AA}$  absorption line has opposite sign to that of the emission lines in a given spectrum; and (3) sharp displacement close to zero velocity is exhibited in the forbidden emission lines [OI]  $\lambda 6300\text{\AA}$  and [SII]  $\lambda 6731\text{\AA}$ . The extent of the displacement varies with the ratio F<sub>1</sub>:F<sub>2</sub>, and in fact the relative displacement in the red and blue wings in the emission lines in a given position spectrum also depends upon this ratio. The extent of the displacement dramatically decreases as the slit width becomes smaller (see Figure 3).

The point source geometry depicted in Figure 3 does not provide a good representation of observing conditions, as such the seeing conditions are simulated by convolving the two point sources by use of a gaussian function. The simulated intensity distribution is then described as:

$$F(x, y) = G_1(x, y) + G_2(x, y) \quad (4)$$

where:

$$G_1(x, y) = \frac{2.773}{(FWHM)^2\pi} F_1 e^{-2.773 \frac{(x-\Delta x_1)^2 + (y-\Delta y_1)^2}{(FWHM)^2}}$$

$$G_2(x, y) = \frac{2.773}{(FWHM)^2\pi} F_2 e^{-2.773 \frac{(x-\Delta x_2)^2 + (y-\Delta y_2)^2}{(FWHM)^2}}$$

where FWHM is the full width half maximum of the seeing profile, ( $\Delta x_1$ ,  $\Delta y_1$ ) is the position of the primary point source, ( $\Delta x_2$ ,  $\Delta y_2$ ) the position of the secondary point source, F<sub>1</sub> and F<sub>2</sub> are the flux of primary and secondary point sources respectively. Combining equations (3) & (4) results in:

$$X_{cent}(\lambda) = \frac{\int \int x F(x, y) f(\lambda + \Delta\lambda(y)) dx dy}{\int \int F(x, y) f(\lambda + \Delta\lambda(y)) dx dy} \quad (5)$$

The two point sources, having being allocated the relevant relative flux, are convolved by our simplified model of the seeing and subsequently shifted according to equation 2. A position spectrum is then obtained as described by equation 5

A simulated position spectrum (Figure 4), obtained as described above, shows displacement on a scale smaller than those artefacts obtained by the unconvolved point source.

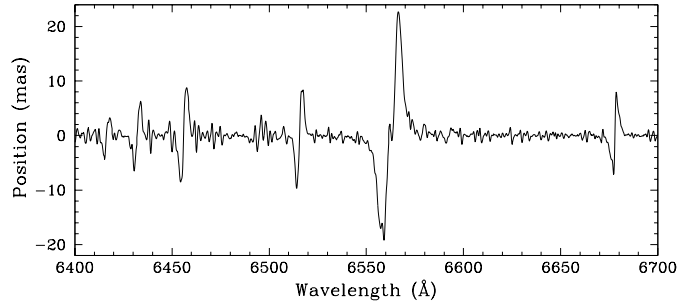


**Figure 4.** Position spectrum obtained as described in §3.1, where the parameters slit width, seeing  $\Delta S_{distort}$  and F<sub>distort</sub> are 1.0'', 0.8'', 0.7'' and 0.5 respectively.

This is because much of the light falls close to and on the center of the slit and as such suffers less of a “shift”. In this instance a 1.0'' slit is simulated with FWHM of 0.8'', as was the case for those observations shown in Figure 1. The two point sources were defined 0.7'' apart, with equal flux (i.e. F<sub>1</sub>:F<sub>2</sub> = 1) and both off center of the slit, as described in Figure 3. The angular scale of the displacement simulated for H $\alpha$  emission ( $\sim 25\text{mas}$ ) compares well with the artefacts observed in the position spectra obtained at the NTT.

In order to investigate the limitations imposed on spectro-astrometry due to systematic effects, the extent of the artefacts that can be expected when uneven illumination of the slit occurs (perhaps due to tracking errors or instrumental concerns) for a given set of conditions is simulated. A single point source is allocated at the centre of the slit with flux F<sub>1</sub> and subsequently convolved by use of a gaussian function. A distortion in the resulting PSF is simulated by “relocating” a percentage of the flux attributed to the point source (F<sub>distort</sub>) to a new position off centre of the slit. The results of these simulations are shown in Figure 6, in which the full extent of the artificial signal, measured from peak to trough, is shown for a range of seeing, slit width, distance between the “real image” and distortion ( $\Delta S_{distort}$ ) and the amount of flux attributed to the distortion (F<sub>distort</sub>), the values of which are given in Table 1. The results are shown for an F<sub>distort</sub> of 0.1 and 1.0 for given slit widths and  $\Delta S_{distort}$ . From this we can clearly see that for small  $\Delta S_{distort}$  where the distortion in the PSF cannot be detected by eye artificial spectro-astrometric signal is still generated on a scale  $\sim 5\text{mas}$  in H $\alpha$ , above the typical detection limit of 1mas for previous spectro-astrometric observations (Takami 2001,

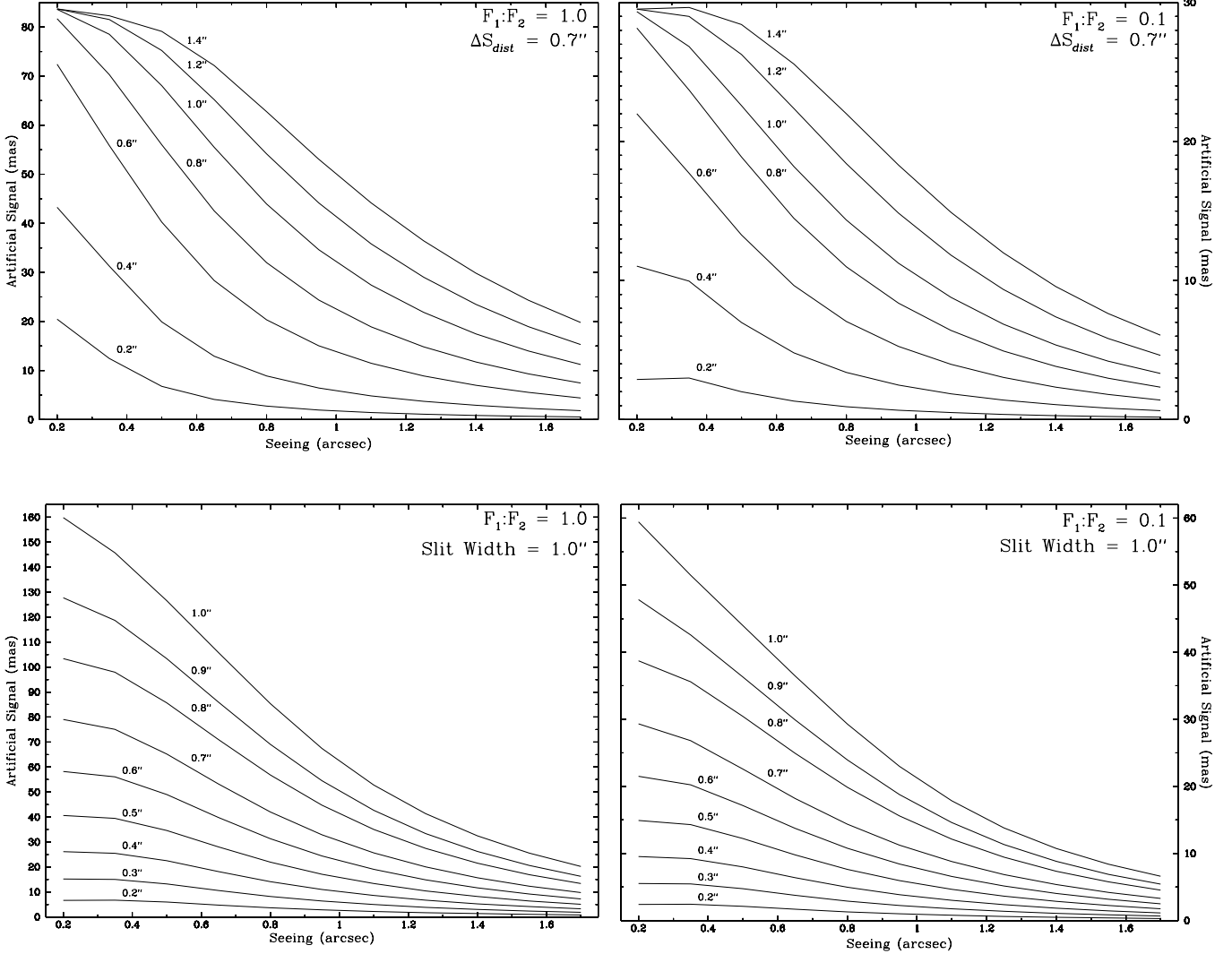


**Figure 5.** Simulated angular displacement in  $H\alpha$ , measured from peak to trough, for a range of seeing, slit width, distance between the “real image” and distortion ( $\Delta S_{distort}$ ) and the amount of flux attributed to the distortion ( $F_{distort}$ , which gives the ratio  $F_1:F_2$ ), the values of which are given in Table 1. Top: Artificial signal generated for a given slit width (solid lines) for a range of seeing values, with  $F_1:F_2=1.0$  (left) and  $F_1:F_2=0.1$  (right). Bottom: Artificial signal generated for a given separation between “real image” and distortion,  $\Delta S_{distort}$  (solid lines) for a range of seeing values, with  $F_1:F_2=1.0$  (left) and  $F_1:F_2=0.1$  (right).

2003). In fact when the input parameters are similar to the conditions during earlier observations described in Takami 2001, 2003 (i.e. seeing  $1.5''$  coupled with a slit width of  $1.0''$ ) the displacement in  $H\alpha$  shows an angular scale of  $\sim 7 - 8$  mas, similarly above the typical detection limit. Therefore it is imperative to obtain data at anti-parallel slit angles in order to determine, by qualitative inspection, if any detected signal is in fact from a real structure in the object, even when the PSF appears symmetric.

The model suggests that the effect can be minimised by defocusing the telescope. For example, Figure 5 shows that given a slit width of  $1.0''$  an increase of 50% in the seeing parameter (from  $0.8''$  to  $1.2''$ ) results in a reduction of the angular scale of the simulated artefacts by a factor of 2. However, the use of a slit width narrow in comparison to the seeing reduces the extent of the artefacts to a greater extent. From Figure 5 it can be seen that given a seeing of

$0.8''$  a decrease in the slit width by 50% (from  $1.0''$  to  $0.5''$ ) results in a reduction of the angular scale of the simulated artefacts by a factor of 3. As such it is clear that a reduction in the slit width is the best option in order to minimise the magnitude of these artefacts.

### 3.2 Binary Simulations

In order to determine (1) what, if any, effect the use of a relatively narrow slit might have on the detection of any real spectro-astrometric signal from the object, and (2) how this systematic effect will affect real signals from the object, the convolved model was adapted with the introduction of an artificial binary companion. The intensity spectrum allocated to the secondary binary component is the same as that in the primary with line to continuum ratio increased by a factor of 2 in order to allow a “real” spectro-astrometric

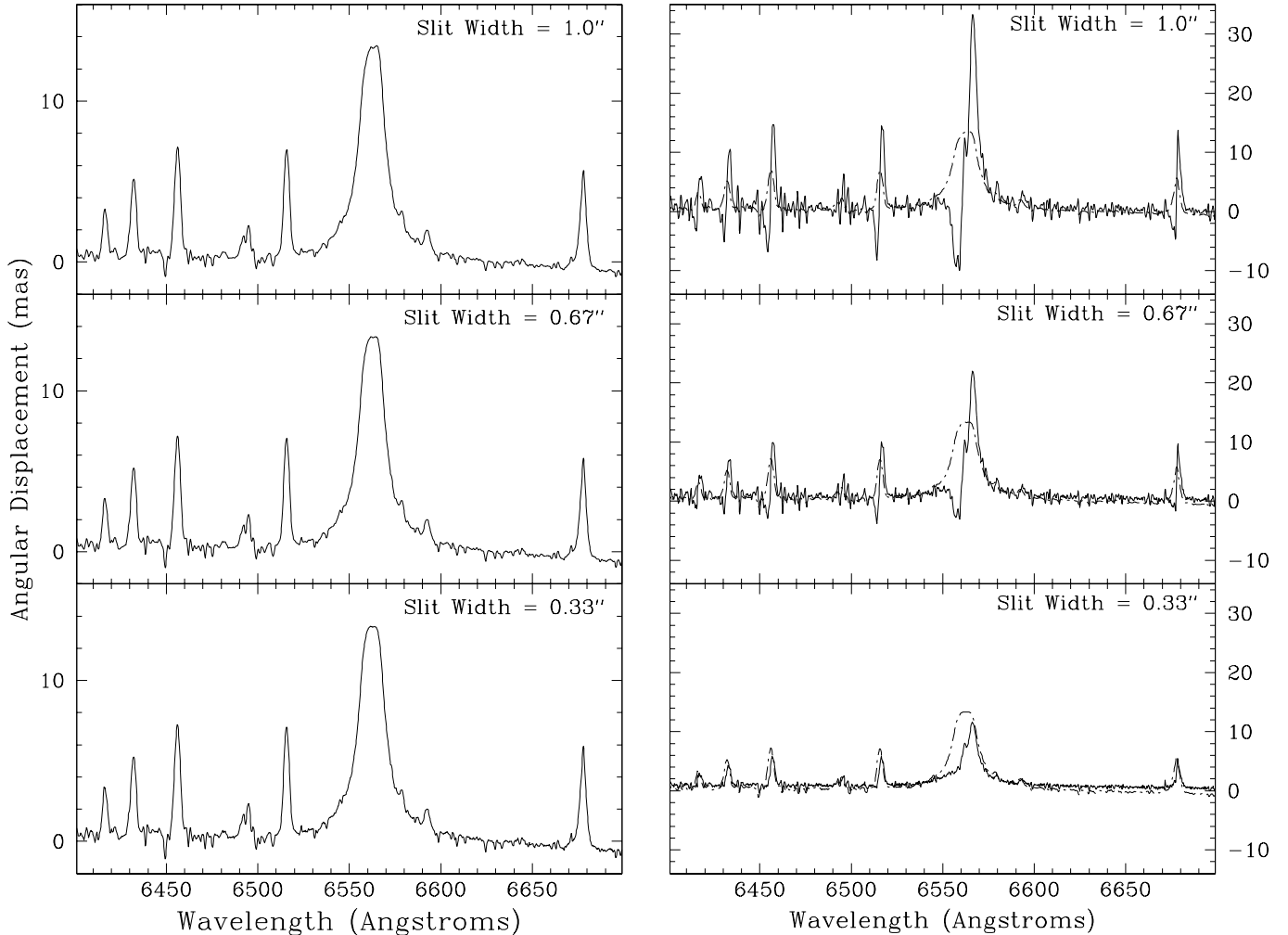


**Figure 6.** Binary simulations with (right) and without (left) a distorted PSF. The true displacement is represented by a dot-dashed line in the left panel. A range of slit widths are displayed in each case: 1.0'', 0.67'' & 0.33'' (top to bottom respectively).

signal to be detected in the simulated binary object, the parameters used in these simulations are listed in Table 1. A percentage of the binary flux is allocated to a distortion in the PSF to simulate the effect of “uneven illumination”.

Figure 6 shows an example result of the simulations when no distortion is present, the parameters for the position spectra shown are those given in Table 1, the specific values of  $F_{\text{distort}}$ ,  $\Delta S_{\text{distort}}$  and seeing (FWHM) are 0.5, 0.7'' and 0.8'' respectively. From this figure we can see that the “real” spectro-astrometric signal is unaffected by a reduction in slit width, therefore the use of a narrow slit has a minimal effect on the extent of the real signal from the object and must therefore be an efficient method of reducing the artificial displacement in the observed position spectra.

Also shown in Figure 6 is both the spectro-astrometric signal detected when the PSF suffered distortion, and the “real” spectro-astrometric signal that is detected when the PSF suffers no distortion (dot-dashed line). The simulations show that the extent of the detected artefacts is reduced by a factor of  $\sim 1.5$  when the slit width is reduced by a third (from 1'' to 0.67''), and when the slit width is reduced by two thirds (from 1'' to 0.33'') the artefacts are reduced by

a factor of  $\sim 3$ . Caveat: the use of a slit width smaller than the seeing will result in the loss of photons. As such, the measured positional accuracy is affected by the reduction in slit width (see Takami 2003). For example, if the slit width is reduced by a factor of 2 the number of photons detected ( $N$ ) will reduce the signal to noise ( $\propto N^2$ ) by a factor of 4, resulting in a reduction in the detection limit ( $\propto N^{-1/2}$ ), and hence the positional accuracy achieved, by a factor of 2.

#### 4 CONCLUSIONS AND RECOMMENDATIONS

Artificial spectro-astrometric signal can be produced in a position spectrum as a result of a distorted stellar image in a relatively wide slit, as was the case in data obtained using the 3.6m NTT. The observed artificial displacement looks similar to that produced when observing an object exhibiting bipolar structure, the only difference being that a real signal from bipolar structure will change sign when

observed using anti-parallel slit position angles whereas the artificial signal will not.

Time variable distortion of the stellar image is a significant problem, the time variation seen is presumably due to variation of the PSF, and as such the resulting magnitude of the effect is time-averaged. As a result the artefacts cannot be removed by subtracting position spectra obtained using long slit spectra with anti-parallel slit position angles, as is the case for other instrumental effects. Spectro-astrometric data must therefore be carefully monitored during observations to determine when these artefacts arise and the observations adjusted to compensate.

Simulations show that the use of a slit width narrow in comparison to the seeing greatly reduces the extent of this instrumental effect. However, an image of high quality and good tracking of the telescope are mandatory in order to obtain position spectra with high positional accuracy.

Based on observations and simulations we recommend that in order to minimise these artefacts and obtain position spectra with high positional accuracy the following are taken into account:

(i) When observing use a slit width narrow in comparison to the seeing. This systematic effect was not observed in observations where the seeing is typically  $1.5''$  -  $2.0''$  and the slit width used was  $1.0''$ .

(ii) The use of an integral field unit (IFU) may be advantageous as they do not experience uneven illumination (e.g. IFU's with micro lenses or fibres), however although previous work by Garcia et al. (1999) appear to have been successful, instrumental effects arising in IFU's may well be more complicated than those from long slit spectrographs. These should be investigated.

(iii) Obtain spectra with a wide spectral range. The systematic effect will create the same artificial signal in a number of emission and absorption features. Therefore if a wide spectral range is observed to include a number of absorption and emission lines with a range of excitations it will be possible to deduce if the bipolar signal is real.

(iv) Spectra should be obtained at anti-parallel slit position angles. Not all instrumental effects are well understood or anticipated, as such comparison of position spectra obtained using anti-parallel slit position angles is the best method to determine whether or not the signal detected is due to real structure in the source.

## ACKNOWLEDGMENTS

We acknowledge the data analysis facilities provided by the Starlink Project which is run by CCLRC on behalf of PPARC. EB and MT thank PPARC for support through a post-grad studentship and PDRA respectively. This research has made use of the NASA's Astrophysics Data System Abstract Service.

## REFERENCES

Aime C., Borgnino J., Lund G., Ricort G. 1988, Conference on High-Resolution Imaging by Interferometry: Ground-Based Interferometry at Visible and Infrared

Wavelengths, Garhing Bei München, Germany, Mar. 15-18, 1988. Edited by F. Merkle, ESO Conference and Workshop Proceedings No. 29, p249, 1988, 249  
 Bailey J.A. 1998a, Proc. SPIE, 3355, 932  
 Bailey J. 1998b, Mon. Not. R. Ast. Soc., 301, 161  
 Baines D. et al. 2004, Mon. Not. R. Ast. Soc., 272  
 Beckers J.M., 1982, Opt. Acta, 29, 361  
 Boss A.P., Yorke H.W., 1993, ApJ, 411, L99  
 Boss A.P., Yorke H.W., 1996, ApJ, 469, 366  
 Chiang E.I., Goldreich P. 1999, ApJ, 519, 279  
 Davis C.J., Ray T.P., Desroches L., Aspin C. 2001, Mon. Not. R. Ast. Soc., 326, 524  
 Davis C.J., Whelan E., Ray T.P., Chrysostomou A. 2003, A&A, 397, 693 PASP, 97, 616  
 Dougados C., Bouvier J., Duvert G., Garcia P.J.V., Folha D.F.M. 2003, Ap&SS, 286, 151  
 Eisloffel J., Mundt R., Ray T.P., Rodriguez L.F. 2000, Protostars and Planets IV, 815  
 Garcia P.J.V., Thiébaud E., Bacon R. 1999, A&A, 346, 892  
 Hirth G.A., Mundt R., Solf J. 1997, A&AS, 126, 437  
 Lago M.T.V.T., Penston M.V. 1982, Mon. Not. R. Ast. Soc., 198, 429  
 Lin D.N.C., Papaloizou J.C.B. 1993, Protostars and Planets III, 749  
 Marconi A., Maiolino R., Petrov R.G. 2003, Ap&SS, 286, 245  
 Petrov R.G. & The AMBER Consortium 2003, Ap&SS, 286, 57  
 Sorokin L.Y., Tokovinin A.A. 1985, Sov. Astron. Lett. 11, 226  
 Solf J., Böhm K.H. 1993, ApJ, 410, L31  
 Takami M., Bailey J., Chrysostomou A. 2003, A&A, 397, 675  
 Takami M., Bailey J., Gledhill T.M., Chrysostomou A., Hough J.H. 2001, Mon. Not. R. Ast. Soc., 323, 177  
 Takami M., Chrysostomou A., Bailey J., Gledhill T.M., Tamura M., Terada H. 2002, ApJ, 568, L53  
 Whelan, E.T., Ray T.P., Davis C.J. 2004, A&A, 417, 247

## APPENDIX A: PREVIOUS RESULTS REPORTED BY TAKAMI ET AL. (2001, 2003)

The detection of bipolar outflows in  $H\alpha$  has been reported previously in RU Lup and CS Cha, Takami et al. (2001); Takami, Bailey & Chrysostomou (2003) respectively, see Figure A1. In order to confirm that the results reported are due to real signals from the objects and not to the artefacts described in this work the (previously unpublished) anti-parallel slit data, which do not show the effect, are included in Figure A1.

Displacement from the centroidal continuum position is seen in both objects at  $H\alpha$   $\lambda 6563\text{\AA}$ , and additionally at [SII]  $\lambda 6716, 6731\text{\AA}$  and [NII]  $\lambda 6584\text{\AA}$  in RU Lup. Figure A1 clearly shows that spectro-astrometric signal detected in anti-parallel slits ( $0^\circ - 180^\circ$ ,  $90^\circ - 270^\circ$ ) are displaced in opposing directions indicating a genuine signal from the object. In addition, the blueshifted  $H\alpha$  wing in RU Lup is displaced in the same direction as the forbidden emission, a well known probe for outflowing gas. The position angle of the displacement for  $H\alpha$  emission for CS Cha is perpendicular to the optical continuum polarisation, which is very often perpendicu-



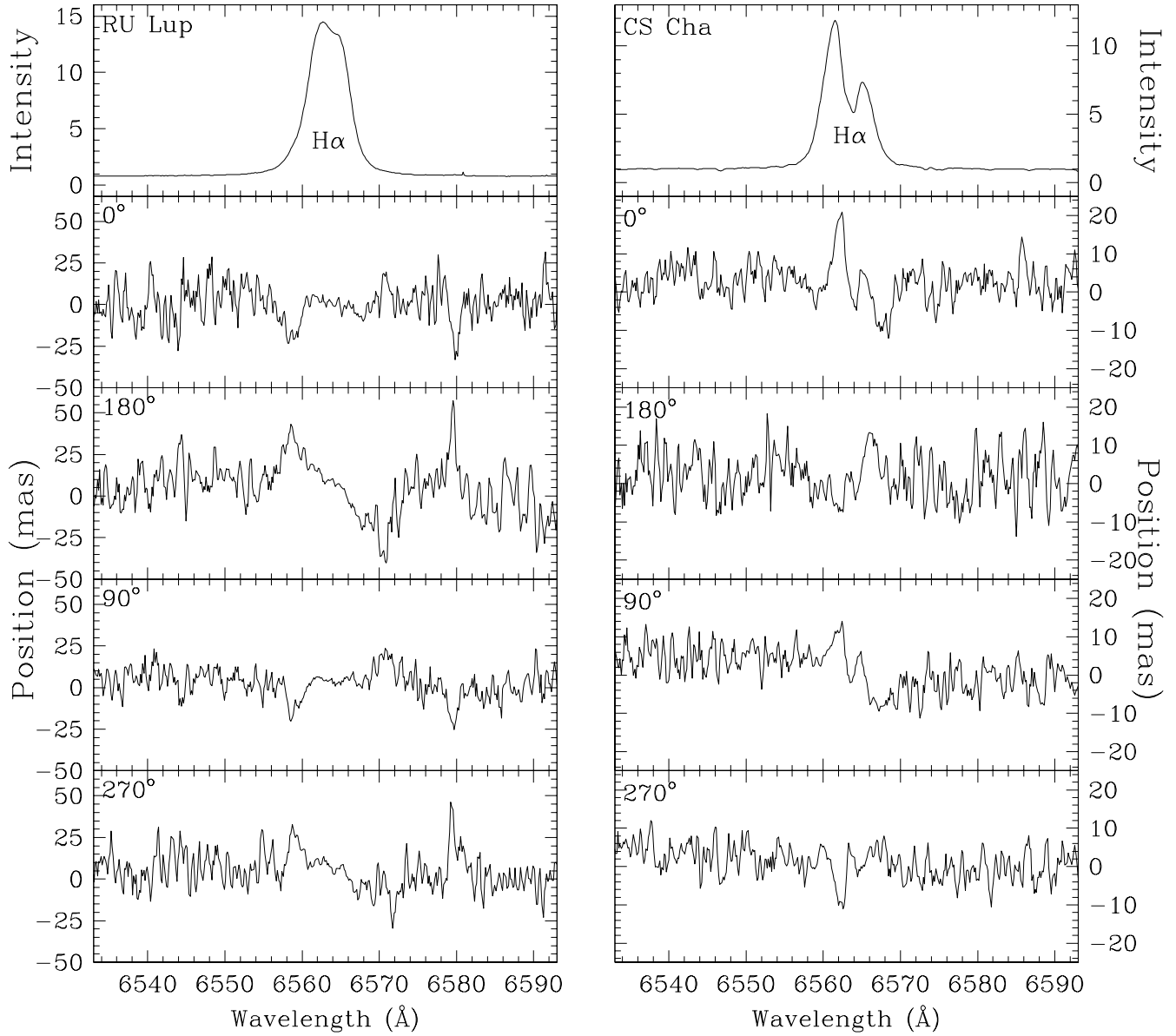


**Figure A1.** Intensity and position spectra ( $H\alpha$ ) of RU Lup (left) and CS Cha (right) reported in Takami (2001) and Takami (2003) respectively. Position spectra for each object were obtained at position angles of  $0^\circ$ ,  $90^\circ$ ,  $180^\circ$  &  $270^\circ$ .

lar to the jet axis (Takami, Bailey & Chrysostomou (2003)). We thus conclude that the results reported by Takami et al. (2001); Takami, Bailey & Chrysostomou (2003) are real and not artefacts.

This paper has been typeset from a  $\text{T}_{\text{E}}\text{X}/\text{L}^{\text{A}}\text{T}_{\text{E}}\text{X}$  file prepared by the author.

# On The Detection of Artefacts in Spectro-Astrometry

E.Brannigan<sup>1\*</sup>, M. Takami<sup>1,2</sup>, A. Chrysostomou<sup>1</sup>, J. Bailey<sup>3</sup>

<sup>1</sup> *Centre for Astrophysics Research, University of Hertfordshire, Hatfield, HERTS AL10 9AB, UK*

<sup>2</sup> *Subaru Telescope, 650 North A'ohoku Place, Hilo, HI 96720, USA*

<sup>3</sup> *Anglo-Australian Observatory, PO Box 296, Epping, NSW 1710, Australia*

Accepted 2005 ??, Received ????, in original form ????

## ABSTRACT

We demonstrate that artificial bipolar structure can be detected using spectro-astrometry when the point spread function (PSF) of a point source suffers distortion in a relatively wide slit. Spectro-Astrometry is a technique which allows us to probe the spatial structure of astronomical sources on milliarcsecond (mas) scales making it possible to detect close binaries and to study the geometry and kinematics of outflowing gas on scales much smaller than the seeing or the diffraction limit of the telescope. It is demonstrated that distortion of the PSF, caused by tracking errors of the telescope or unstable active optics during an exposure can induce artificial signals which may be misinterpreted as a real spectro-astrometric signal. Using simulations we show that these may be minimised by using a narrow slit relative to the seeing. Spectra should be obtained at anti-parallel slit position angles (e.g.,  $0^\circ$  and  $180^\circ$ ) for comparison in order to allow artificial signatures to be identified.

**Key words:** Spectro-Astrometry Line: Formation Line: Profiles Stars: Pre-Main Sequence ISM: Jets and Outflows.

## 1 INTRODUCTION

Spatial resolutions of optical-IR facilities have dramatically improved over the last decade. Indeed, the *Hubble Space Telescope* and adaptive optics on ground based 8-10m telescopes have provided spatial resolutions of 0.05 arcseconds, leading to a better understanding of the nature of a variety of astronomical objects. Despite this, even higher spatial resolutions are desired to study the geometry of extrasolar planetary systems, populations and formation of close binaries, mechanisms of mass ejection and accretion in young and evolved stars and the nature of active galactic nuclei. Optical-IR interferometry has begun to provide resolutions on milliarcsecond (mas) scales, however its applicability is limited due to the complexity of the technique.

Spectro-astrometry is an alternative approach to study milliarcsecond structures at optical-IR wavelengths. The basic concept is to measure the relative position of the source as a function of wavelength using either an intensity weighted centroiding algorithm or profile fitting (see Bailey 1998a for a more detailed description). The resultant “position spectrum” will show structure on any spectral feature that is displaced from the centroid of the continuum source: e.g., an emission line arising in a binary companion, outflowing jets or any other structure that is not perfectly symmetric about the centroidal source, or whose displacement from the

source varies with wavelength. The smallest spatial scale observed is limited by the seeing or the diffraction limit of the telescope, however this technique indeed provides astronomically useful information at spatial scales much smaller than these.

The concept was introduced in the 1980's as “Differential Speckle Interferometry” or “Chromatic Position Difference” (e.g., Beckers 1982), and demonstrated to detect close binaries (e.g., Sorokin & Tokovinin 1985). This broad band technique was limited by the necessity to correct for atmospheric dispersion which can be much larger than the observed structure. This difficulty is removed by measuring the displacement of a spectral line at high resolution. Aime et al. (1988) were able to measure spectro-astrometric structure using special instrumentation. See Bailey (1998a) for review of these works.

More recently Bailey (1998a) adapted this technique using a standard long-slit CCD spectrograph and coined the term “spectro-astrometry”. The method is similar to that used by Solf & Böhm (1993), who studied a jet from a young stellar object (YSO) on subarcsecond/arcsecond scales. Bailey (1998a) revised this method and has shown that with good spatial uniformity of the CCD coupled with a pixel scale that allows excellent sampling of the seeing profile positional accuracies as small as 1mas are achieved (see Takami 2003). Bailey has also shown that the technique is a powerful tool for discovering binary companions toward young and evolved stars, separating their spectra, and study-

\* E-mail: e.brannigan@star.herts.ac.uk

ing the kinematics of YSO jets/winds and narrow line regions of active galactic nuclei (AGN). Since this method doesn't require any special instrumentation, its popularity has steadily increased in recent years. Studies made for young binaries and YSO jets include Bailey (1998b), Takami et al. (2001,2002,2003), Davis et al. (2001,2003), Whelan, Ray & Davis (2004) and Baines et al. (2004). Measurements using an integral field unit (IFU) were first conducted by Garcia, Thiébaud & Bacon (1999). A similar approach using VLT-AMBER is investigated by Petrov (2003), Marconi et al. (2003) and Dougados et al. (2003). Since the positional accuracy achieved depends on the PSF size as well as the photon noise, using an interferometer for this approach has the potential to achieve information on spatial structures at *microarcsecond* scales (Bailey 1998a).

Instrumental effects which may compromise spectroastrometric observations have not been fully investigated. These effects may indeed create false detections of close binaries or bipolar outflows. Possible instrumental effects include; misalignment of the spectrum with CCD columns, any departure of the CCD pixels from a regular grid, imperfect flatfielding or charge transfer deficiencies in the CCD (Bailey 1998b; Takami et al. 2001). To eliminate instrumental effects, Bailey (1998a,b) proposed to obtain position spectra at anti-parallel slit position angles (e.g.,  $0^\circ$  and  $180^\circ$ ) via rotation of the instrument. On comparison of these spectra, any real signal from the object will change sign, while the instrumental effects remain constant. We can thus eliminate instrumental effects by subtracting one position spectrum from the other. This method is followed by Takami et al. (2001,2002,2003) and Baines (2004). Garcia et al. (1999), Davis et al. (2001,2003) and Whelan et al. (2004) however eliminate instrumental effects by polynomial fitting of the continuum position.

Bailey (1998a) reports a systematic effect upon observation of sharp unresolved lines. This is caused by either telescope tracking errors or unstable active optics during the exposure, and appears in the position spectrum as a P Cygni type profile. Bailey warns that the target spectral lines should be well resolved to observe true positional displacement. This instrumental effect could be eliminated in some cases by Bailey's method, but this cannot be done by polynomial fitting of the continuum position. In this paper we show that this instrumental effect can appear even if the line profile is fully resolved as was the case in position spectra of RU Lupi, obtained using the 3.5m New Technology Telescope (NTT). Takami et al. had previously detected the presence of bipolar outflow in this object using the 3.9m Anglo-Australian Telescope (AAT). Indeed the observed positional displacement in the NTT looks similar to that seen in the AAT data. We show that the signal detected in the NTT data is not real, motivating us to investigate the effect of uneven illumination on spectro-astrometry, how to avoid it and whether previously detected bipolar outflows are in fact real.

In §2 we describe the spectro-astrometric observations obtained using EMMI on the 3.6m NTT and the results in which artificial signatures were detected. These artefacts are identified by qualitatively inspecting position spectra obtained using anti-parallel slit position angles. In §3 we (1) show that the observed position spectra are explained by distortion/motion of the stellar image in a relatively wide

slit, (2) show that the extent of the artefacts, in a given set of observing conditions, can be greatly reduced by using a slit width narrow in comparison to the seeing, and (3) show an example of the effect these artefacts have on real spectroastrometric data. In §4 we give some recommendations on how to monitor the data for the false signatures of bipolar structure. In Appendix A, we show that the bipolar outflows reported by Takami et al. (2001,2003) are real and not due to the instrumental effect described here.

## 2 OBSERVATIONS AND RESULTS

Medium resolution spectroscopy of RU Lup was obtained with the 3.5m NTT in the early morning of April 8 2004, when the seeing was measured to be  $0.8''$ . The observations were made using the REad Medium Dispersion (REMD) mode of the ESO Multi-Mode Instrument (EMMI) with the #6 grating and an arcsecond slit. The wavelength coverage spanned 6100 to 6800Å with resolving power = 5000. The spectra were obtained at 4 position angles:  $0^\circ$ ,  $90^\circ$ ,  $180^\circ$ ,  $270^\circ$  by rotating the instrument. HeAr lamp spectra were used to calibrate the wavelength scale and a pixel scale of  $0.165''$  with the MIT detector provided good sampling of the seeing profile. Flat fields were obtained by combining many exposures of the spectrograph illuminated by a halogen lamp.

The data were reduced using the FIGARO package provided by Starlink, following Bailey (1998a,b) and Takami (2001,2003). After subtracting the bias level and flatfielding, "position spectra" were determined by fitting the seeing profile at each wavelength with a gaussian function. Global instrumental effects in the position spectra are removed by polynomial fitting. This allows us to see the positional displacement of any emission/absorption features at each slit angle relative to the continuum. In addition to the position spectra, the intensity spectra were obtained by subtracting the bias, flat-fielding, subtracting the adjacent sky and extracting bright columns on the CCD.

The spectrum of RU Lup shows a wealth of emission lines as observed by Lago & Penston (1982) and Takami (2001). The intensity and position spectra of the  $H\alpha$   $\lambda 6563\text{\AA}$ , HeI  $\lambda 6678\text{\AA}$  & [SII]  $\lambda 6731\text{\AA}$  emission lines and LiI  $\lambda 6708\text{\AA}$  absorption line, obtained using EMMI-NTT, are shown in Figure 1. The  $H\alpha$  emission line shows a large offset in the position spectrum,  $\sim 25\text{mas}$  from the continuum position and the blue and red shifted wings are displaced in different directions. Similar displacement in  $H\alpha$  is reported in Takami (2001). Such structure usually indicates the presence of a bipolar outflow (see Appendix A). However a qualitative inspection of position spectra, obtained using anti-parallel slits (i.e.  $0^\circ$  &  $180^\circ$ ) in this data, reveals that the displacement seen in anti-parallel position spectra have equal sign indicating that the signature must be systematic. In addition, the displacement observed with slit position angle  $0^\circ$  is less than that observed with position angle  $180^\circ$ . In fact two position spectra observed at a position angle of  $0^\circ$  exhibit dissimilar profiles indicating that the effect responsible for the spurious displacement signal is time variable and as such cannot be removed even by obtaining position spectra at anti-parallel slit angles.

In addition to  $H\alpha$   $\lambda 6563\text{\AA}$  and HeI  $\lambda 6678\text{\AA}$ , evidence for

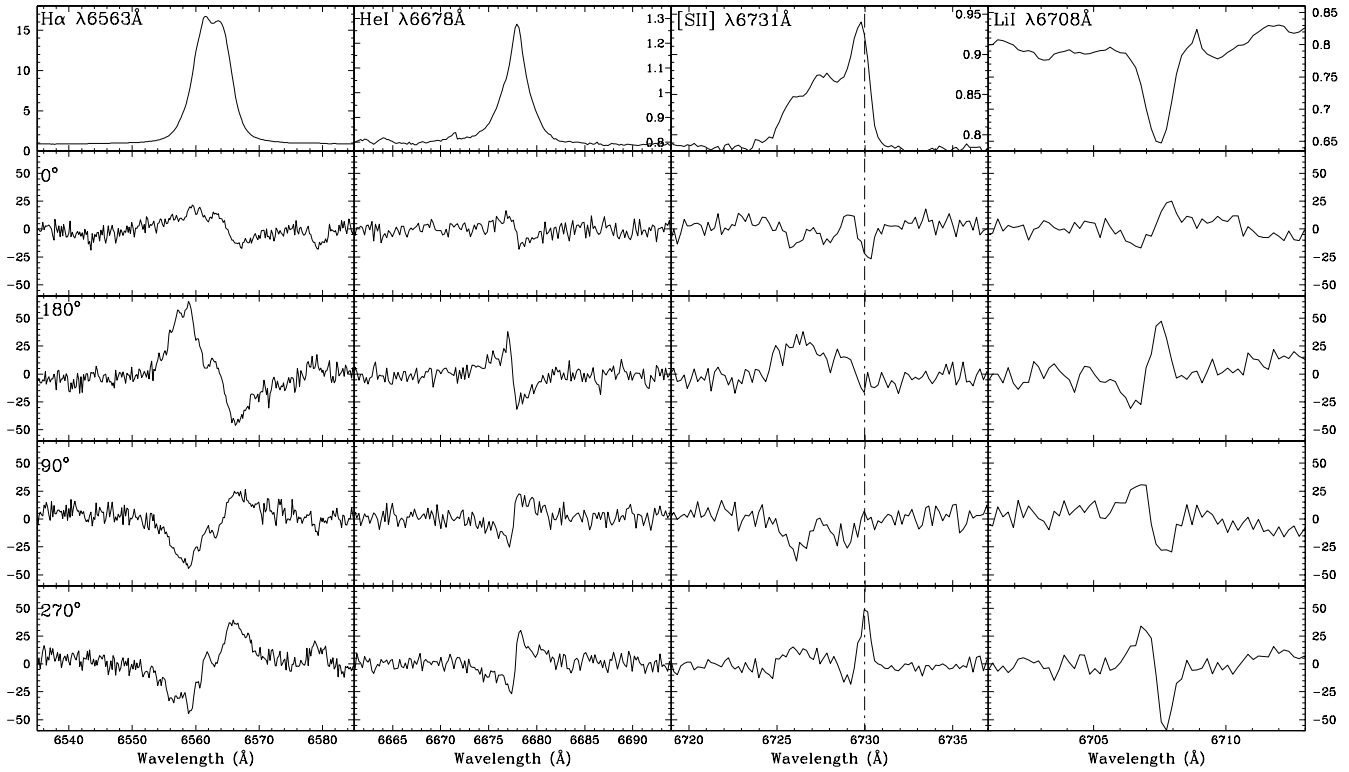


**Figure 1.** Intensity and position spectra of RU Lup obtained using EMMI-NTT. From left to right; Top: H $\alpha$   $\lambda$ 6563Å, HeI  $\lambda$ 6678Å & [SII]  $\lambda$ 6731Å emission and LiI  $\lambda$ 6708Å absorption lines. The intensities shown are arbitrary; Lower four panels: spectro-astrometric signal (mas) for each corresponding spectral feature detected at 4 position angles  $0^\circ$ ,  $180^\circ$ ,  $90^\circ$  &  $270^\circ$  in the spectrum of RU Lup. The bottom two panels show position spectra for anti-parallel slit angles  $90^\circ$  &  $270^\circ$  in each of the spectral features, similarly in the third and fourth panels from the bottom position spectra for anti-parallel slit angles  $0^\circ$  &  $180^\circ$  in each of the spectral features is shown. In the blue wing of [SII]  $\lambda$ 6731Å emission feature the angular displacement is seen to change sign in corresponding anti-parallel slits, whereas displacement near zero velocity of the [SII]  $\lambda$ 6731Å line (marked with a dot-dashed line), in the permitted emission lines and the LiI  $\lambda$ 6708Å absorption line does not change sign in anti-parallel slits.

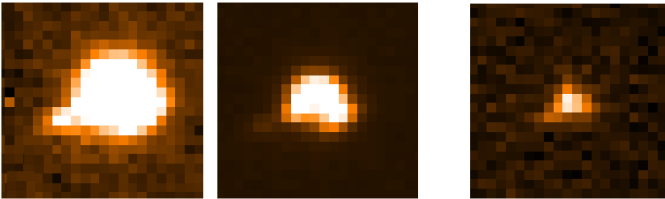


**Figure 2.** Image capture in slit viewer 7/4/2004 using 3.5m NTT. Pixel scale:  $0.4''$ . Left and Centre: distorted image of the Classical T Tauri Star (CTTS) SZ68. Right: distorted image of the CTTS SZ69

bipolar structure is seen in other bright permitted lines including FeII  $\lambda$ 6238/6248/6456/6516Å. The LiI  $\lambda$ 6708Å absorption line exhibits displacement similar to that of H $\alpha$  and the bright permitted emission lines, although in any given spectrum the direction of displacement in Li I absorption is of opposite sign to that of the emission lines. For example, at a position angle of  $180^\circ$  the blue and redshifted components of the bright permitted emission lines show positive and negative displacement respectively, whereas the Li I absorption line shows negative and positive displacement in the blue and red wings respectively.

Conversely, the direction of displacement due to

blueshifted forbidden line emission reverses sign at anti-parallel slit positions ( $0^\circ$  vs.  $180^\circ$ ;  $90^\circ$  vs.  $270^\circ$ ). This is best seen in the [SII]  $\lambda$ 6731Å emission line in Figure 1. However a large, sharp displacement is observed close to zero velocity in the position spectrum at both [SII]  $\lambda$ 6731Å and [OI]<sup>1</sup>  $\lambda$ 6300Å emission lines. This displacement is observed in all the position spectra for [SII]  $\lambda$ 6731Å (marked in Figure 1 with a dot-dashed line) and [OI]  $\lambda$ 6300Å. This sharp displacement does not reverse sign in anti-parallel slit position angles and therefore this is likely to be due to instrumental effects and not to actual signal from the object.

### 3 INDUCED SIGNAL DUE TO A DISTORTED STELLAR IMAGE IN A WIDE SLIT

The instrumental effects described in §2 were not observed in previous observing runs at the AAT described in Takami et al. (2001,2003). There are a number of key differences between these earlier observations and those reported in §2. Primarily, the typical seeing conditions differ dramatically ( $0.8''$  and  $1.5''/2.0''$ ) while a wide slit of  $1.0''$  was used in

<sup>1</sup> not shown as the effect in this line is the same as that in the [SII] line, but the data at the wavelength of [OI] is of lower quality

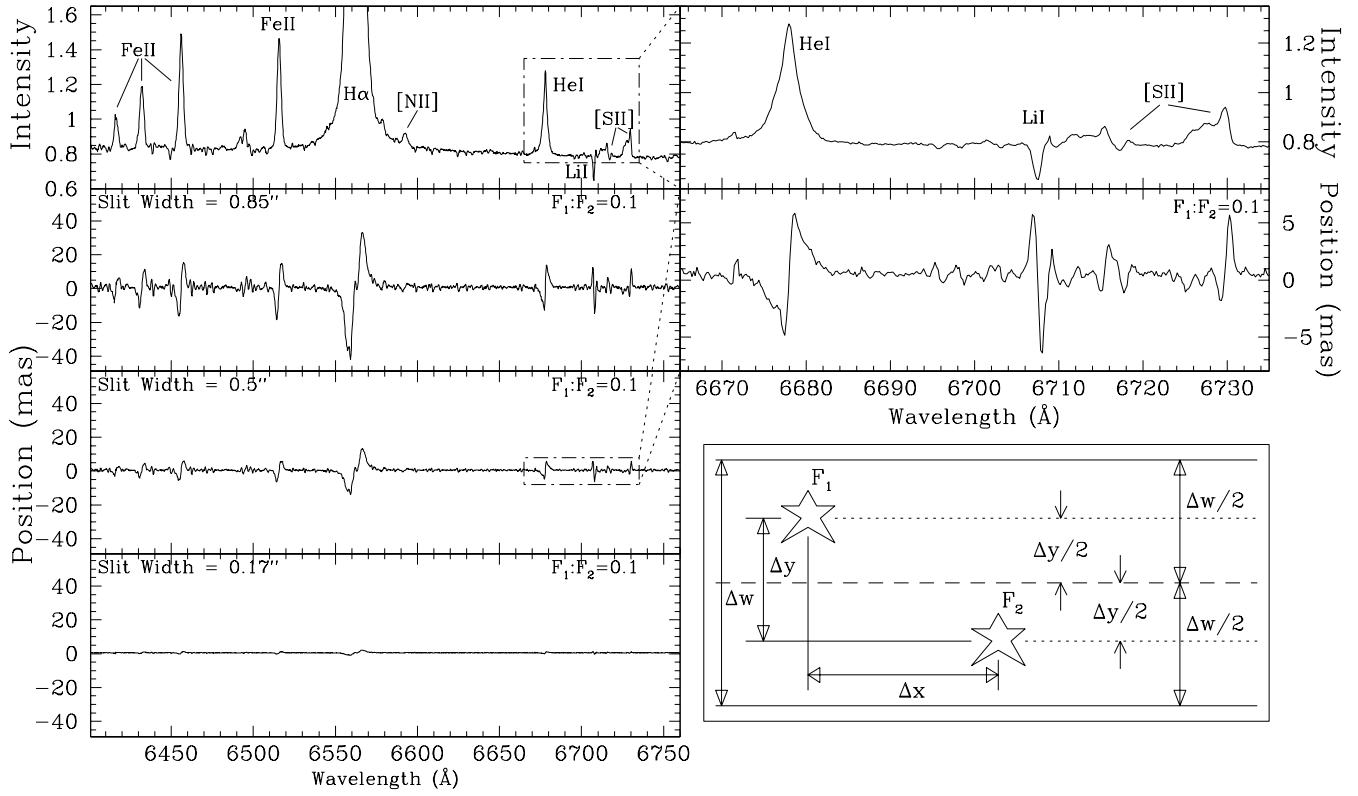


**Figure 3.** Top left: Intensity spectrum of RU Lup obtained on 8/4/2004 using EMMI on the 3.6m NTT. Lower left: simulated position spectra for a distorted PSF using 3 slit widths, 0.85'', 0.5'' & 0.17'', flux ratio  $F_1 : F_2 = 0.1$  and two point sources located off centre of the slit with identical spectra. Lower right: geometry used in the simulations to show that a distorted PSF can reproduce well the artefacts seen in the data. Top right: Close up view of the HeI, [SII] and LiI emission and absorption lines. Lower top right: positional displacement due to HeI, [SII] and LiI obtained from the simulations, where  $F_1 : F_2 = 0.1$  and slit width = 0.5''. The simulated displacement is similar to that seen in the data.

all of the observations. These artefacts are seen in observations when the seeing is smaller than the slit width used. Secondly, the stellar image suffered intermittent distortion during the later observations, as shown in Figure 2, due to an unstable active optics system. In §3.1 it is explained how these combined effects can induce an artificial signal in the position spectrum, and the extent of the artefacts that can be expected to occur for a given set of observing conditions is investigated. In §3.2 an example of the effect these artefacts can have on real spectro-astrometric signal is simulated.

### 3.1 Concepts and Simulations

When the intensity distribution from a given source is non-uniform across the slit the resultant spectrum can be slightly blue or redshifted. This blue/redshifted emission due to “uneven illumination” or “inaccurate centering”, (e.g., Bacciotti et al. 2002; Ardila et al. 2002) arises from an offset of the light source from the center of the slit, resulting in a deviation of the angle of incidence according to  $d\alpha = dy/f_{col}$ , where  $f_{col}$  is the focal length of the collimator. According to the grating equation:

$$m\lambda = (\sin \alpha \pm \sin \beta) \quad (1)$$

where  $m$  is the diffracted order,  $\lambda$  the diffracted wavelength,  $\alpha$  is the angle of incidence wrt. the normal and  $\beta$  the angle of diffraction wrt. the normal, this leads to a subsequent

deviation in the angle of diffraction which in turn is translated to a shift in the spectrum. Therefore, the shift in the spectrum,  $d\lambda$ , is proportional to the position of the light source from the center of the slit axis  $dy$ ;  $d\lambda = \text{const.} \times dy$ . This constant value can be readily determined from the spectral resolution of the instrument. For the REMD mode of EMMI-NTT a 1.0'' slit provides  $R = 5000$ , corresponding to  $\Delta\lambda = 1.2\text{\AA}$  giving us the relation:

$$d\lambda [\text{\AA}] = 1.2 \times dy [\text{arcsec}] \quad (2)$$

As such, if a stellar image is distorted or elongated in the slit, perhaps due to tracking errors of the telescope or unstable active optics, the spectrum close to the edges of the slit is slightly blue or redshifted. This geometry would be replicated by a bipolar outflow located within the slit. In order to determine the affect of these artefacts on spectro-astrometric observations simplified simulations of two point sources were carried out with their positions as depicted in Figure 3. Given that the point sources have spectra  $F_1 f(\lambda)$  and  $F_2 f(\lambda)$ , where  $F_1$  and  $F_2$  are constant and  $f(\lambda)$  is a normalised spectrum, the spectra are recorded at the detector as  $F_1 f(\lambda + \Delta\lambda)$  and  $F_2 f(\lambda - \Delta\lambda)$ . Thus the centroidal position at each wavelength is given by:

$$X_{cent}(\lambda) = \frac{\Delta x}{2} \times \frac{F_1 f(\lambda + 1.2\Delta y) - F_2 f(\lambda - 1.2\Delta y)}{F_1 f(\lambda + 1.2\Delta y) + F_2 f(\lambda - 1.2\Delta y)} \quad (3)$$

Parameter	Description	Distortion	Binary	Binary & Distortion
PS	Pixel Scale	0.17	0.17	0.17
$\lambda_{min}$	start wavelength	6100	6100	6100
$\lambda_{max}$	end wavelength	6850	6850	6850
$PA_{bin}$	Binary position angle	—	45°	45°
$\Delta S_{bin}$	Binary separation	—	0.1''	0.1''
$F_1$	Flux of primary binary component	1.0	3.0	3.0
$F_2$	Flux of secondary binary component	—	1.0	1.0
$F_{distort}$	Percentage of flux in distortion	0.1 - 0.9	—	0.1 - 0.9
$PA_{distort}$	Distortion position angle	135°	—	135°
$\Delta S_{distort}$	Distance between distortion and “real image”	0.1'' - 1.0''	—	0.1'' - 1.0''
FWHM	Gaussian simulated seeing	0.2'' - 1.7''	0.2'' - 1.7''	0.2'' - 1.7''
$\Delta w$	Slit width	0.1'' - 1.4''	0.1'' - 1.4''	0.1'' - 1.4''

**Table 1.** Parameters used in the simulations.

To confirm that the artefacts seen in this data are a result of uneven illumination of the slit simulations of a distorted PSF were carried out and position spectra obtained using equation (3), and the geometry described in Figure 3. The simulations reproduce a number of the artefacts observed in the data (Figure 1), specifically (see Figure 3): (1) evidence for bipolar structure exists in the bright permitted emission lines; (2) displacement seen at the Li I  $\lambda 6708\text{\AA}$  absorption line has opposite sign to that of the emission lines in a given spectrum; and (3) sharp displacement close to zero velocity is exhibited in the forbidden emission lines [OI]  $\lambda 6300\text{\AA}$  and [SII]  $\lambda 6731\text{\AA}$ . The extent of the displacement varies with the ratio  $F_1:F_2$ , and in fact the relative displacement in the red and blue wings in the emission lines in a given position spectrum also depends upon this ratio. The extent of the displacement dramatically decreases as the slit width becomes smaller (see Figure 3).

The point source geometry depicted in Figure 3 does not provide a good representation of observing conditions, as such the seeing conditions are simulated by convolving the two point sources by use of a gaussian function. The simulated intensity distribution is then described as:

$$F(x, y) = G_1(x, y) + G_2(x, y) \quad (4)$$

where:

$$G_1(x, y) = \frac{2.773}{(FWHM)^2\pi} F_1 e^{-2.773 \frac{(x-\Delta x_1)^2 + (y-\Delta y_1)^2}{(FWHM)^2}}$$

$$G_2(x, y) = \frac{2.773}{(FWHM)^2\pi} F_2 e^{-2.773 \frac{(x-\Delta x_2)^2 + (y-\Delta y_2)^2}{(FWHM)^2}}$$

where FWHM is the full width half maximum of the seeing profile,  $(\Delta x_1, \Delta y_1)$  is the position of the primary point source,  $(\Delta x_2, \Delta y_2)$  the position of the secondary point source,  $F_1$  and  $F_2$  are the flux of primary and secondary point sources respectively. Combining equations (3) & (4) results in:

$$X_{cent}(\lambda) = \frac{\int \int x F(x, y) f(\lambda + \Delta\lambda(y)) dx dy}{\int \int F(x, y) f(\lambda + \Delta\lambda(y)) dx dy} \quad (5)$$

The two point sources, having being allocated the relevant relative flux, are convolved by our simplified model of the seeing and subsequently shifted according to equation 2. A position spectrum is then obtained as described by equation 5

A simulated position spectrum (Figure 4), obtained as described above, shows displacement on a scale smaller than those artefacts obtained by the unconvolved point source.

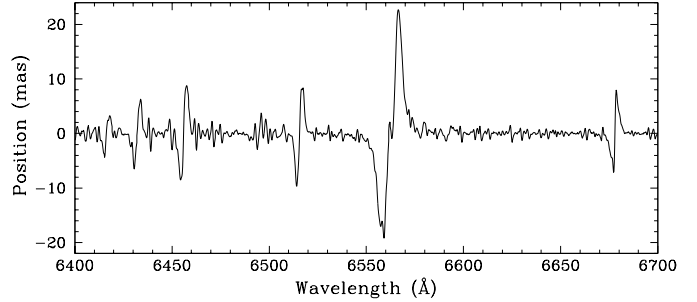


**Figure 4.** Position spectrum obtained as described in §3.1, where the parameters slit width, seeing  $\Delta S_{distort}$  and  $F_{distort}$  are 1.0'', 0.8'', 0.7'' and 0.5 respectively.

This is because much of the light falls close to and on the center of the slit and as such suffers less of a “shift”. In this instance a 1.0'' slit is simulated with FWHM of 0.8'', as was the case for those observations shown in Figure 1. The two point sources were defined 0.7'' apart, with equal flux (i.e.  $F_1:F_2 = 1$ ) and both off center of the slit, as described in Figure 3. The angular scale of the displacement simulated for H $\alpha$  emission ( $\sim 25\text{mas}$ ) compares well with the artefacts observed in the position spectra obtained at the NTT.

In order to investigate the limitations imposed on spectro-astrometry due to systematic effects, the extent of the artefacts that can be expected when uneven illumination of the slit occurs (perhaps due to tracking errors or instrumental concerns) for a given set of conditions is simulated. A single point source is allocated at the centre of the slit with flux  $F_1$  and subsequently convolved by use of a gaussian function. A distortion in the resulting PSF is simulated by “relocating” a percentage of the flux attributed to the point source ( $F_{distort}$ ) to a new position off centre of the slit. The results of these simulations are shown in Figure 6, in which the full extent of the artificial signal, measured from peak to trough, is shown for a range of seeing, slit width, distance between the “real image” and distortion ( $\Delta S_{distort}$ ) and the amount of flux attributed to the distortion ( $F_{distort}$ ), the values of which are given in Table 1. The results are shown for an  $F_{distort}$  of 0.1 and 1.0 for given slit widths and  $\Delta S_{distort}$ . From this we can clearly see that for small  $\Delta S_{distort}$  where the distortion in the PSF cannot be detected by eye artificial spectro-astrometric signal is still generated on a scale  $\sim 5\text{mas}$  in H $\alpha$ , above the typical detection limit of 1mas for previous spectro-astrometric observations (Takami 2001,

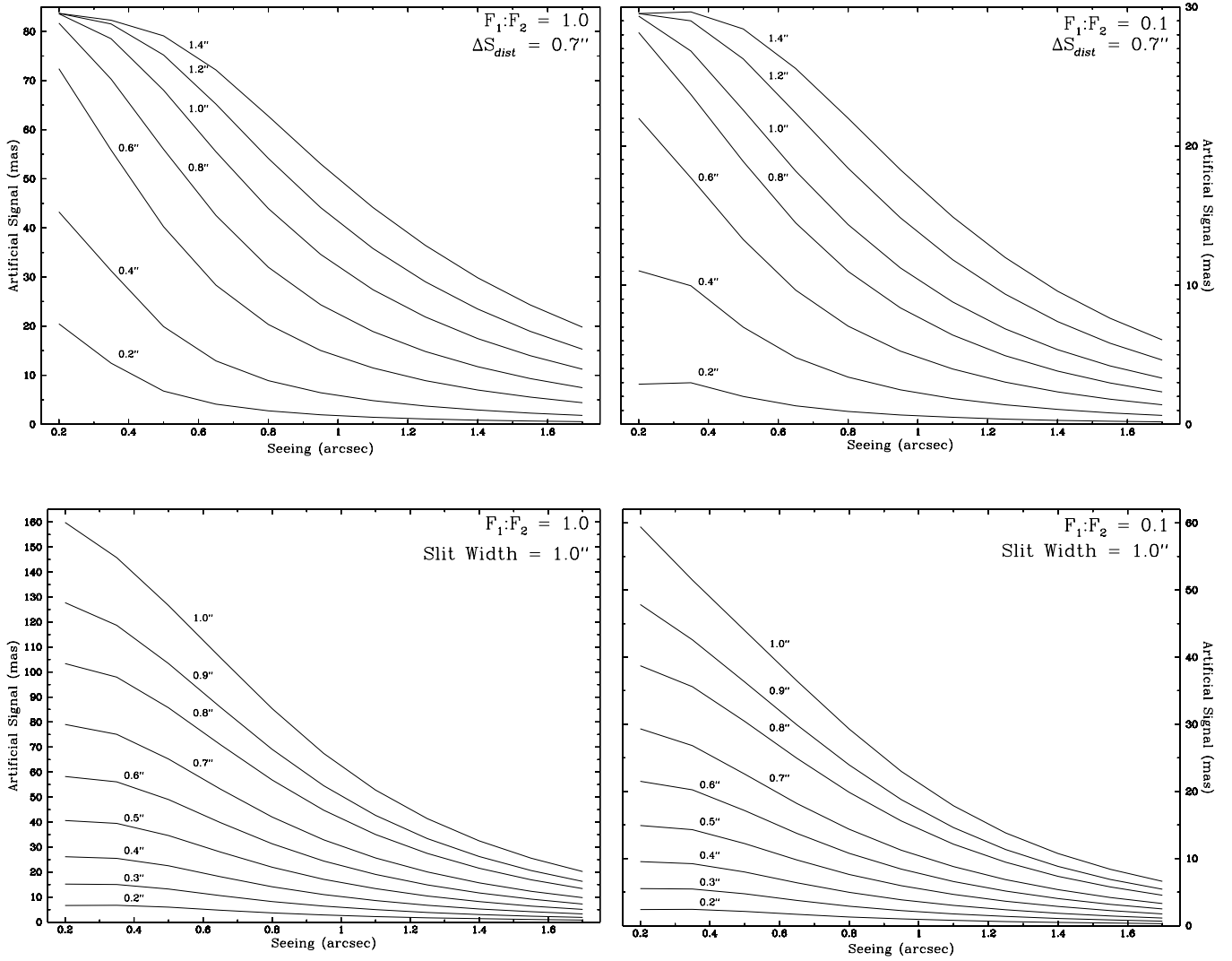


**Figure 5.** Simulated angular displacement in  $H\alpha$ , measured from peak to trough, for a range of seeing, slit width, distance between the “real image” and distortion ( $\Delta S_{distort}$ ) and the amount of flux attributed to the distortion ( $F_{distort}$ , which gives the ratio  $F_1:F_2$ ), the values of which are given in Table 1. Top: Artificial signal generated for a given slit width (solid lines) for a range of seeing values, with  $F_1:F_2=1.0$  (left) and  $F_1:F_2=0.1$  (right). Bottom: Artificial signal generated for a given separation between “real image” and distortion,  $\Delta S_{distort}$  (solid lines) for a range of seeing values, with  $F_1:F_2=1.0$  (left) and  $F_1:F_2=0.1$  (right).

2003). In fact when the input parameters are similar to the conditions during earlier observations described in Takami 2001, 2003 (i.e. seeing  $1.5''$  coupled with a slit width of  $1.0''$ ) the displacement in  $H\alpha$  shows an angular scale of  $\sim 7 - 8$  mas, similarly above the typical detection limit. Therefore it is imperative to obtain data at anti-parallel slit angles in order to determine, by qualitative inspection, if any detected signal is in fact from a real structure in the object, even when the PSF appears symmetric.

The model suggests that the effect can be minimised by defocusing the telescope. For example, Figure 5 shows that given a slit width of  $1.0''$  an increase of 50% in the seeing parameter (from  $0.8''$  to  $1.2''$ ) results in a reduction of the angular scale of the simulated artefacts by a factor of 2. However, the use of a slit width narrow in comparison to the seeing reduces the extent of the artefacts to a greater extent. From Figure 5 it can be seen that given a seeing of

$0.8''$  a decrease in the slit width by 50% (from  $1.0''$  to  $0.5''$ ) results in a reduction of the angular scale of the simulated artefacts by a factor of 3. As such it is clear that a reduction in the slit width is the best option in order to minimise the magnitude of these artefacts.

### 3.2 Binary Simulations

In order to determine (1) what, if any, effect the use of a relatively narrow slit might have on the detection of any real spectro-astrometric signal from the object, and (2) how this systematic effect will affect real signals from the object, the convolved model was adapted with the introduction of an artificial binary companion. The intensity spectrum allocated to the secondary binary component is the same as that in the primary with line to continuum ratio increased by a factor of 2 in order to allow a “real” spectro-astrometric

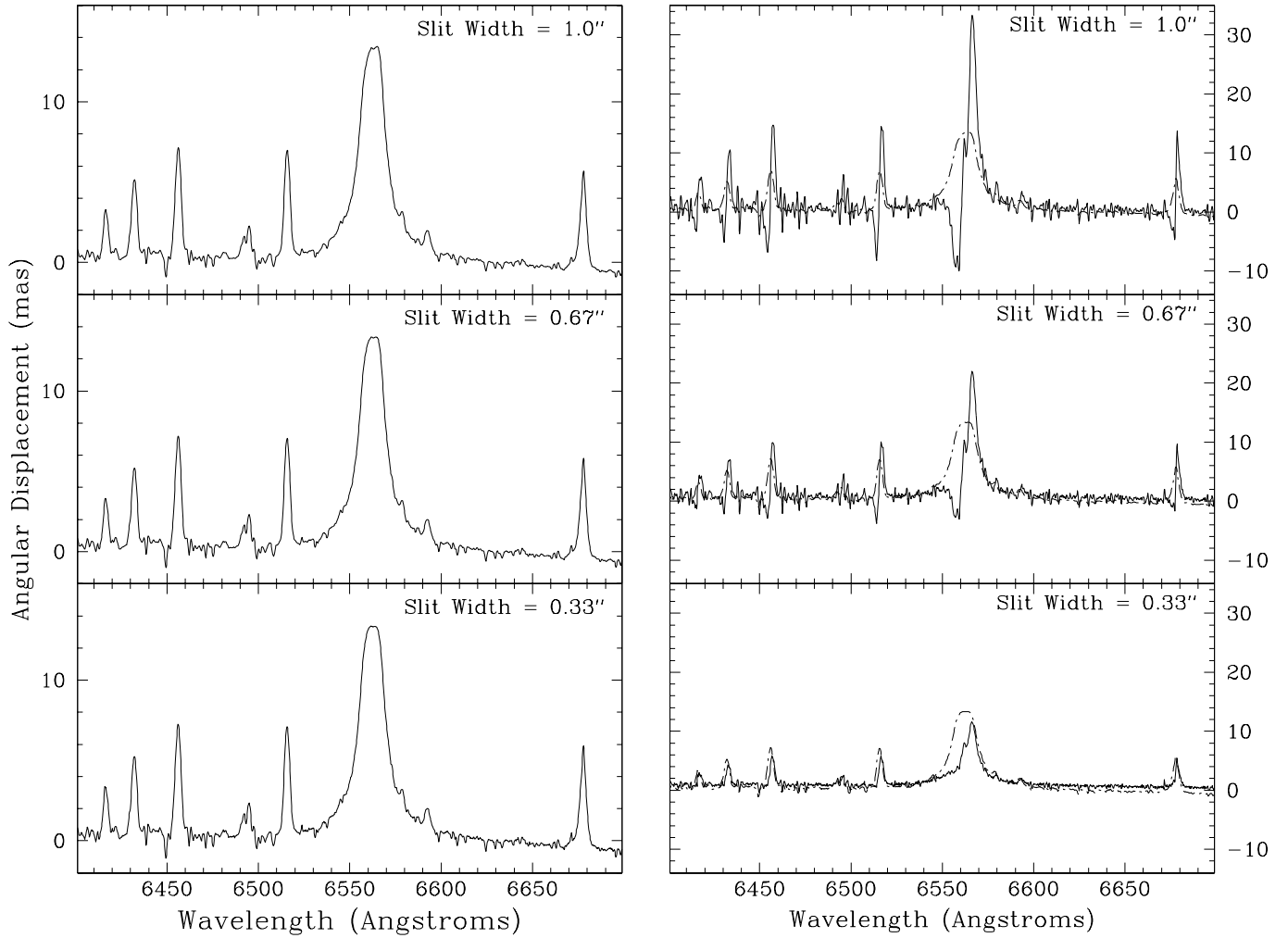


**Figure 6.** Binary simulations with (right) and without (left) a distorted PSF. The true displacement is represented by a dot-dashed line in the left panel. A range of slit widths are displayed in each case:  $1.0''$ ,  $0.67''$  &  $0.33''$  (top to bottom respectively).

signal to be detected in the simulated binary object, the parameters used in these simulations are listed in Table 1. A percentage of the binary flux is allocated to a distortion in the PSF to simulate the effect of “uneven illumination”.

Figure 6 shows an example result of the simulations when no distortion is present, the parameters for the position spectra shown are those given in Table 1, the specific values of  $F_{distort}$ ,  $\Delta S_{distort}$  and seeing (FWHM) are 0.5,  $0.7''$  and  $0.8''$  respectively. From this figure we can see that the “real” spectro-astrometric signal is unaffected by a reduction in slit width, therefore the use of a narrow slit has a minimal effect on the extent of the real signal from the object and must therefore be an efficient method of reducing the artificial displacement in the observed position spectra.

Also shown in Figure 6 is both the spectro-astrometric signal detected when the PSF suffered distortion, and the “real” spectro-astrometric signal that is detected when the PSF suffers no distortion (dot-dashed line). The simulations show that the extent of the detected artefacts is reduced by a factor of  $\sim 1.5$  when the slit width is reduced by a third (from  $1''$  to  $0.67''$ ), and when the slit width is reduced by two thirds (from  $1''$  to  $0.33''$ ) the artefacts are reduced by

a factor of  $\sim 3$ . Caveat: the use of a slit width smaller than the seeing will result in the loss of photons. As such, the measured positional accuracy is affected by the reduction in slit width (see Takami 2003). For example, if the slit width is reduced by a factor of 2 the number of photons detected ( $N$ ) will reduce the signal to noise ( $\propto N^2$ ) by a factor of 4, resulting in a reduction in the detection limit ( $\propto N^{-1/2}$ ), and hence the positional accuracy achieved, by a factor of 2.

#### 4 CONCLUSIONS AND RECOMMENDATIONS

Artificial spectro-astrometric signal can be produced in a position spectrum as a result of a distorted stellar image in a relatively wide slit, as was the case in data obtained using the 3.6m NTT. The observed artificial displacement looks similar to that produced when observing an object exhibiting bipolar structure, the only difference being that a real signal from bipolar structure will change sign when



observed using anti-parallel slit position angles whereas the artificial signal will not.

Time variable distortion of the stellar image is a significant problem, the time variation seen is presumably due to variation of the PSF, and as such the resulting magnitude of the effect is time-averaged. As a result the artefacts cannot be removed by subtracting position spectra obtained using long slit spectra with anti-parallel slit position angles, as is the case for other instrumental effects. Spectro-astrometric data must therefore be carefully monitored during observations to determine when these artefacts arise and the observations adjusted to compensate.

Simulations show that the use of a slit width narrow in comparison to the seeing greatly reduces the extent of this instrumental effect. However, an image of high quality and good tracking of the telescope are mandatory in order to obtain position spectra with high positional accuracy.

Based on observations and simulations we recommend that in order to minimise these artefacts and obtain position spectra with high positional accuracy the following are taken into account:

(i) When observing use a slit width narrow in comparison to the seeing. This systematic effect was not observed in observations where the seeing is typically  $1.5''$  -  $2.0''$  and the slit width used was  $1.0''$ .

(ii) The use of an integral field unit (IFU) may be advantageous as they do not experience uneven illumination (e.g. IFU's with micro lenses or fibres), however although previous work by Garcia et al. (1999) appear to have been successful, instrumental effects arising in IFU's may well be more complicated than those from long slit spectrographs. These should be investigated.

(iii) Obtain spectra with a wide spectral range. The systematic effect will create the same artificial signal in a number of emission and absorption features. Therefore if a wide spectral range is observed to include a number of absorption and emission lines with a range of excitations it will be possible to deduce if the bipolar signal is real.

(iv) Spectra should be obtained at anti-parallel slit position angles. Not all instrumental effects are well understood or anticipated, as such comparison of position spectra obtained using anti-parallel slit position angles is the best method to determine whether or not the signal detected is due to real structure in the source.

## ACKNOWLEDGMENTS

We acknowledge the data analysis facilities provided by the Starlink Project which is run by CCLRC on behalf of PPARC. EB and MT thank PPARC for support through a post-grad studentship and PDRA respectively. This research has made use of the NASA's Astrophysics Data System Abstract Service.

## REFERENCES

Aime C., Borgnino J., Lund G., Ricort G. 1988, Conference on High-Resolution Imaging by Interferometry: Ground-Based Interferometry at Visible and Infrared

Wavelengths, Garhing Bei München, Germany, Mar. 15-18, 1988. Edited by F. Merkle, ESO Conference and Workshop Proceedings No. 29, p249, 1988, 249  
 Bailey J.A. 1998a, Proc. SPIE, 3355, 932  
 Bailey J. 1998b, Mon. Not. R. Ast. Soc., 301, 161  
 Baines D. et al. 2004, Mon. Not. R. Ast. Soc., 272  
 Beckers J.M., 1982, Opt. Acta, 29, 361  
 Boss A.P., Yorke H.W., 1993, ApJ, 411, L99  
 Boss A.P., Yorke H.W., 1996, ApJ, 469, 366  
 Chiang E.I., Goldreich P. 1999, ApJ, 519, 279  
 Davis C.J., Ray T.P., Desroches L., Aspin C. 2001, Mon. Not. R. Ast. Soc., 326, 524  
 Davis C.J., Whelan E., Ray T.P., Chrysostomou A. 2003, A&A, 397, 693 PASP, 97, 616  
 Dougados C., Bouvier J., Duvert G., Garcia P.J.V., Folha D.F.M. 2003, Ap&SS, 286, 151  
 Eislöffel J., Mundt R., Ray T.P., Rodriguez L.F. 2000, Protostars and Planets IV, 815  
 Garcia P.J.V., Thiébaud E., Bacon R. 1999, A&A, 346, 892  
 Hirth G.A., Mundt R., Solf J. 1997, A&AS, 126, 437  
 Lago M.T.V.T., Penston M.V. 1982, Mon. Not. R. Ast. Soc., 198, 429  
 Lin D.N.C., Papaloizou J.C.B. 1993, Protostars and Planets III, 749  
 Marconi A., Maiolino R., Petrov R.G. 2003, Ap&SS, 286, 245  
 Petrov R.G. & The AMBER Consortium 2003, Ap&SS, 286, 57  
 Sorokin L.Y., Tokovinin A.A. 1985, Sov. Astron. Lett. 11, 226  
 Solf J., Böhm K.H. 1993, ApJ, 410, L31  
 Takami M., Bailey J., Chrysostomou A. 2003, A&A, 397, 675  
 Takami M., Bailey J., Gledhill T.M., Chrysostomou A., Hough J.H. 2001, Mon. Not. R. Ast. Soc., 323, 177  
 Takami M., Chrysostomou A., Bailey J., Gledhill T.M., Tamura M., Terada H. 2002, ApJ, 568, L53  
 Whelan, E.T., Ray T.P., Davis C.J. 2004, A&A, 417, 247

## APPENDIX A: PREVIOUS RESULTS REPORTED BY TAKAMI ET AL. (2001, 2003)

The detection of bipolar outflows in  $H\alpha$  has been reported previously in RU Lup and CS Cha, Takami et al. (2001); Takami, Bailey & Chrysostomou (2003) respectively, see Figure A1. In order to confirm that the results reported are due to real signals from the objects and not to the artefacts described in this work the (previously unpublished) anti-parallel slit data, which do not show the effect, are included in Figure A1.

Displacement from the centroidal continuum position is seen in both objects at  $H\alpha$   $\lambda 6563\text{\AA}$ , and additionally at [SII]  $\lambda 6716, 6731\text{\AA}$  and [NII]  $\lambda 6584\text{\AA}$  in RU Lup. Figure A1 clearly shows that spectro-astrometric signal detected in anti-parallel slits ( $0^\circ - 180^\circ$ ,  $90^\circ - 270^\circ$ ) are displaced in opposing directions indicating a genuine signal from the object. In addition, the blueshifted  $H\alpha$  wing in RU Lup is displaced in the same direction as the forbidden emission, a well known probe for outflowing gas. The position angle of the displacement for  $H\alpha$  emission for CS Cha is perpendicular to the optical continuum polarisation, which is very often

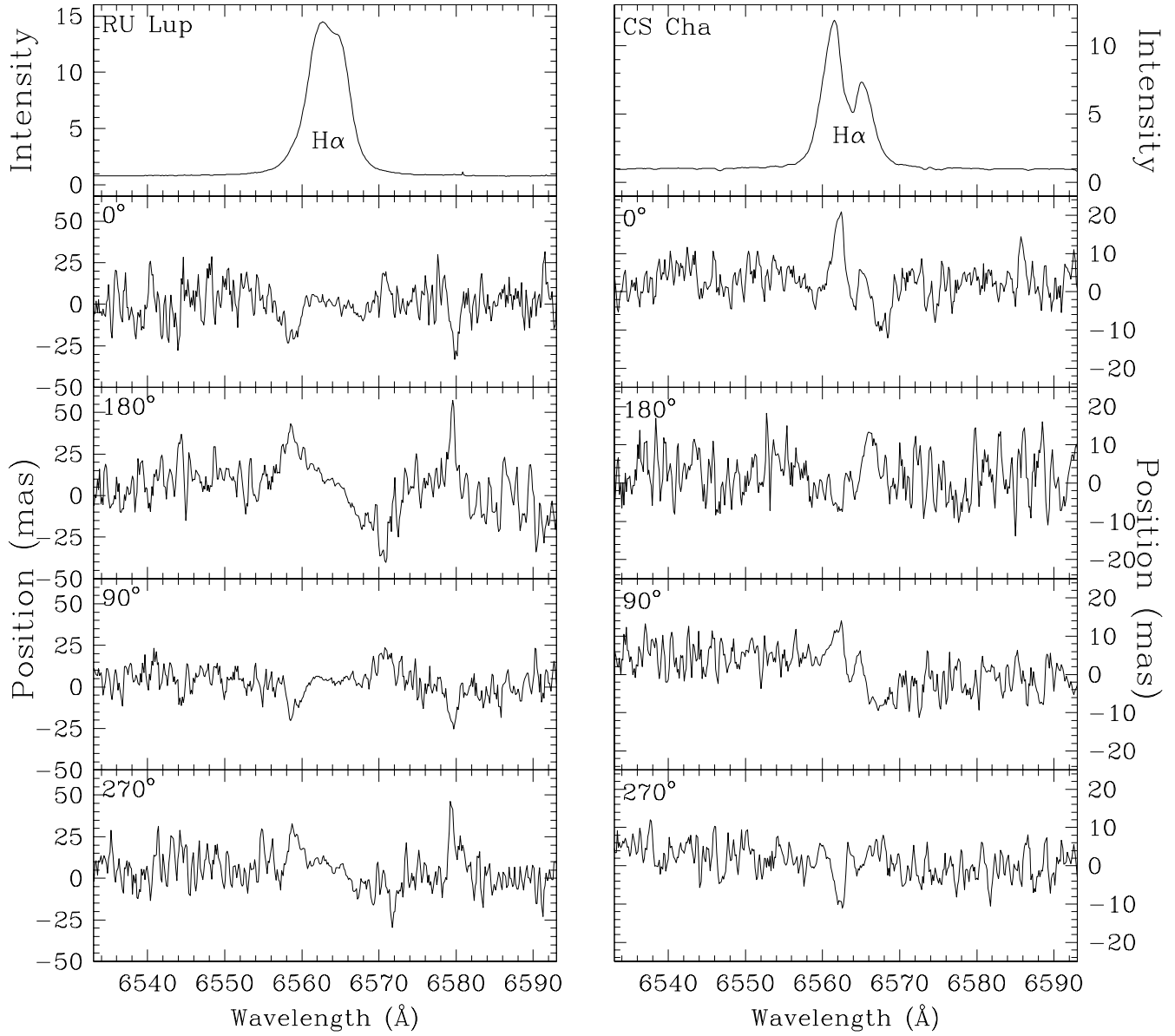


**Figure A1.** Intensity and position spectra ( $H\alpha$ ) of RU Lup (left) and CS Cha (right) reported in Takami (2001) and Takami (2003) respectively. Position spectra for each object were obtained at position angles of  $0^\circ$ ,  $90^\circ$ ,  $180^\circ$  &  $270^\circ$ .

perpendicular to the jet axis (Takami, Bailey & Chrysostomou (2003)). We thus conclude that the results reported by Takami et al. (2001); Takami, Bailey & Chrysostomou (2003) are real and not artefacts.

This paper has been typeset from a  $\text{T}_{\text{E}}\text{X}/\text{L}^{\text{A}}\text{T}_{\text{E}}\text{X}$  file prepared by the author.